Received: 5 May 2023 | Revised: 7 July 2023 | Accepted: 26 August 2023

DOI: 10.1002/hyp.14989

RESEARCH ARTICLE

WILEY

High-resolution in situ stable isotope measurements reveal contrasting atmospheric vapour dynamics above different urban vegetation

Ann-Marie Ring[1,2] | Dörthe Tetzlaff[1,2,3] | Maren Dubbert[4] | David Dubbert[1,4] | Chris Soulsby[3]

[1]Department of Ecohydrology, Leibniz Institute of Freshwater Ecology and Inland Fisheries, Berlin, Germany

[2]Department of Geography, Humboldt University Berlin, Berlin, Germany

[3]Northern Rivers Institute, School of Geosciences, University of Aberdeen, Aberdeen, UK

[4]Research Area 1 "Landscape Processes", Leibniz Institute for Agricultural and Landscape Research, Müncheberg, Germany

Correspondence
Ann-Marie Ring and Dörthe Tetzlaff, Department of Geography, Humboldt University Berlin, Berlin, Germany.
Email: ann-marie.ring@igb-berlin.de and doerthe.tetzlaff@igb-berlin.de

Funding information
Bundesministerium für Bildung und Forschung; Deutsche Forschungsgemeinschaft; Einstein Stiftung Berlin; Leverhulme Trust; German Research Foundation, Grant/Award Number: GRK2032/2; Einstein Research Unit, Grant/Award Number: ERU-2020-609; Einstein Foundation Berlin and Berlin University Alliance; BiNatur, Grant/Award Number: 16LW0156; BMBF, Grant/Award Number: 033W034A; Leverhulme Trust through the ISO-LAND project, Grant/Award Number: RPG 2018 375

Abstract

We monitored stable water isotopes in liquid precipitation and atmospheric water vapour (δ_v) using in situ cavity ring-down spectroscopy (CRDS) over a 2 month period in an urban green space area in Berlin, Germany. Our aim was to better understand the origins of atmospheric moisture and its link to water partitioning under contrasting urban vegetation. δ_v was monitored at multiple heights (0.15, 2 and 10 m) in grassland and forest plots. The isotopic composition of δ_v above both land uses was highly dynamic and positively correlated with that of rainfall indicating the changing sources of atmospheric moisture. Further, the isotopic composition of δ_v was similar across most heights of the 10 m profiles and between the two plots indicating high aerodynamic mixing. Only at the surface at ~0.15 m height above the grassland δ_v showed significant differences, with more enrichment in heavy isotopes indicative of evaporative fractionation especially after rainfall events. Further, disequilibrium between δ_v and precipitation composition was evident during and right after rainfall events with more positive values (i.e., values of vapour higher than precipitation) in summer and negative values in winter, which probably results from higher evapotranspiration and more convective precipitation events in summer. Our work showed that it is technically feasible to produce continuous, longer-term data on δ_v isotope composition in urban areas from in situ monitoring using CRDS, providing new insights into water cycling and partitioning across the critical zone of an urban green space in Central Europe. Such data have the potential to better constrain the isotopic interface between the atmosphere and the land surface and to thus, improve ecohydrological models that can resolve evapotranspiration fluxes.

KEYWORDS
atmospheric vapour isotopes, cities, ecohydrology, equilibrium assumption, in situ monitoring, urban green spaces

1 | INTRODUCTION

Urban green spaces mediate trade-offs between "green" (which sustain vegetation growth and transport water back to the atmosphere) and "blue" (which sustain streamflow and groundwater recharge) water fluxes (Falkenmark & Rockström, 2006). Green spaces have the potential for high evapotranspiration (ET) rates via soil evaporation (E) and plant transpiration (T) (Kool et al., 2014). They potentially mitigate the Urban Heat Island (UHI) effect, but on the other hand might reduce groundwater recharge and stream flow generation (Schirmer et al., 2013). Understanding, quantifying and optimizing this partitioning of E/T across urban critical zones is increasingly important in the face of increased urban growth and climatic warming. In addition, wider benefits of urban green spaces—or green infrastructure—are increasingly recognized; these include the potential to enhance infiltration. and ameliorate urban storm runoff (Ahiablame et al., 2012; Keesstra et al., 2018), to increase local biodiversity (Grimm et al., 2008; Kowarik, 2011), to provide social functions through improved health for local residents (Shashua-Bar et al., 2011; Willis & Petrokofsky, 2017) and to improve water security in terms of sufficient provision of good water quality (Aboelnga et al., 2019; Bichai & Cabrera Flamini, 2018). Consequently, as one component of an evidence base for wider urban planning, the trade-offs between higher ET rates (Gunawardena et al., 2017; Wang et al., 2018) and groundwater recharge (Gillefalk et al., 2021), as well as the linked uncertainties, are an increased focus for research (e.g., BMUB (2018)).

Water stable isotopes have proved valuable tools that can help resolve the partitioning of incoming precipitation into different components of ET fluxes or constrain biosphere-atmosphere feedbacks between atmospheric vapour and ET, and thus have high potential to contribute to a scientific evidence-base for managing urban green spaces (Ehleringer et al., 2016; Kuhlemann et al., 2021). Water isotopes have also been shown to be a useful tracer to understand processes and linkages across the soil–plant–atmosphere continuum in different geographic regions (Dubbert & Werner, 2018; Tetzlaff et al., 2021; Yakir & Sternberg, 2000) although critical zone studies in urban areas are still relatively rare (Marx et al., 2022). The use of isotopes includes tracking the effects of evaporation in isotopic fractionation and identifying the effects of seasonality of water sources for different vegetation types (Oerter & Bowen, 2017; Tetzlaff et al., 2015). Numerous isotope studies have used soil water or river water isotopes to assess evaporative effects (Benettin et al., 2018; Kuhlemann et al., 2021), while others have related the composition of xylem water to potential sources of root water uptake (Marx et al., 2022). However, there is still limited knowledge on subdaily dynamics of ET fluxes (Coenders-Gerrits et al., 2014; Singer et al., 2021), especially from urban vegetation (Meili et al., 2021). These processes can now be quantified with innovative high-resolution in situ measurements of stable water isotopes (Beyer et al., 2020; Rothfuss et al., 2021). However, studies using such high-resolution data to investigate how evaporation and/or transpiration affect the isotopic composition of atmospheric vapour (δ_v) at the surface boundary layer (Berkelhammer et al., 2013; Dubbert et al., 2014; Griffis et al., 2016; Laonamsai et al., 2021; Li et al., 2023; Wei et al., 2019) are especially rare for urban areas (Gorski et al., 2015) and also for elevation profiles above vegetation (Berkelhammer et al., 2013).

The onset of relatively inexpensive cavity ring-down spectroscopes (CRDS) has revolutionized the field of isotope studies allowing efficient tracing of isotopic transformations across the atmospheric water cycle (Galewsky et al., 2016), quantifying ecohydrological interactions (Lee et al., 2005; Werner et al., 2012) and the origin of atmospheric moisture (i.e., evaporation or condensation; Gao et al., 2019). Recent developments in using in situ measurements of stable water isotopes are making use of non-destructive online monitoring techniques and are increasingly advanced (Landgraf et al., 2022; Rothfuss et al., 2021). In terms of analysing δ_v, grab samples or refrigerated traps for offline analysis in the laboratory were already used in the 1990s (Moreira et al., 1997; Walker & Brunel, 1990) with rapidly accelerating progress in recent years (Herbstritt et al., 2022; Magh et al., 2022). Today, CRDS techniques have been shown to be useful for measuring δ_v at continuously high-resolution and thus, enabling real-time analysis of δ_v (Aemisegger et al., 2012; Tremoy et al., 2011; Wei et al., 2015) which can give advanced insights than precipitation alone (Lee et al., 2006). For example, the technique has been successfully deployed for monitoring sub-tropical sub-cloud raindrop evaporation (Li et al., 2020); for testing vapour equilibrium assumption for $\delta^{18}O$ cellulose estimates (Penchenat et al., 2020); for investigating partitioning of evapotranspiration over a rice paddy field (Wei et al., 2015); diurnal and intra-seasonal variations in evaporative signals at different heights above the Greenland ice sheet (Steen-Larsen et al., 2013); and to characterize variation in δ_v and their controlling factors during extreme precipitation events (Xu et al., 2022). To date, however, to our knowledge hardly any in situ studies have assessed δ_v dynamics in the atmospheric boundary of urban green spaces in Central Europe.

Previous isotopic studies have reported contrasting ecohydrological partitioning under different land use types in urban green spaces (Kuhlemann et al., 2021). A study in Scotland assessed land use influences on isotopic variability revealing that urbanization, intensive agriculture and responsive soils caused rapid cycling of precipitation to stream water (Stevenson et al., 2022). Others found higher ET and older groundwater recharge beneath urban trees, but more marked soil evaporative losses under grassland (Gillefalk et al., 2021). By integrating simple modelling and observational water isotope data, Stevenson et al. (2023) quantified the heterogeneities in urban ecohydrological partitioning and found that median ET increased from grassland, to evergreen shrub, to larger deciduous forest through to larger conifer trees, with groundwater recharge behaving contrary. Mixing models applied to different green spaces in Berlin showed that trees were more dependent on deeper, older soil and groundwater sources, whereas grass very probably recycled shallow, younger soil water in transpiration (Marx et al., 2022). Such isotopic information of water fluxes through the critical zone can be used in ecohydrological models that can resolve ET into its component parts. However, to do this, the isotopic gradient at the atmospheric-land surface interface is usually defined in models assuming δ_v is in equilibrium with current or recent rainfall (Gat, 1996; Gat, 2000).

Despite now being logistically possible, monitoring δ_v in situ at different heights and above vegetation canopies is still relatively rare. Braden-Behrens et al. (2019) demonstrated the value of direct in situ eddy covariance measurements of δ_v in the surface boundary layer. Despite standard model assumptions of an equilibrium between δ_v and precipitation, δ_v can be out of equilibrium with local water sources (Fiorella et al., 2019) and can show gradual depletion with altitude (Horita et al., 2008). High-resolution in situ monitoring of δ_v allows testing of such equilibrium assumptions, but so far, very few studies have tested this with in situ ambient data (Mercer et al., 2020; Penchenat et al., 2020).

Here, we conducted a 'proof of concept' study to assess the changing isotopic composition of δ_v and evaporation dynamics over a 2.5 months period in an urban green space with contrasting landcover. We deployed a laser spectrometer in the field for continuous in situ monitoring of δ_v in the urban surface boundary layer. Our overarching research question was whether we can generate data with in situ real-time sequential monitoring to increase our understanding of origins of atmospheric moisture and its link to ET dynamics of contrasting urban vegetation. Our specific objectives were to:

i. Investigate dynamics in δ_v within two contrasting urban vegetation types to understand what types of landcover enhance moisture fluxes back to the atmosphere.
ii. Investigate these changes in relation to related ecohydrological dynamics of soil moisture storage, sap flow rates and biomass accumulation.
iii. Assess the extent of equilibrium between vapour and precipitation.

Based on these assessments, we discuss the future value, challenges and potential in gaining and processing such high-resolution data to improve understanding of ET partitioning at different heights in the atmosphere above different types of landcover in urban green spaces, which would be important for increased process understanding across urban critical zones.

2 | STUDY SITE

The study was carried out in an urban green space in the SE of Berlin, Germany (Figure 1). Berlin is located on the flat North European Plain where the topography and geology are dominated by deposits from the Pleistocene glaciation (Stackebrandt & Manhenke, 2010). The climate is continental temperate with long-term (1991–2020) mean annual rainfall of 579 mm ranging between stations and mean annual air temperatures of 9.6–10.7°C (DWD, 2023b). Berlin covers 891 km^2, with a population of 3.75 million (Amt für Statistik Berlin-Brandenburg, 2023; Figure 1b). The majority of the city is covered by residential areas and streets (~59%), but there are large amounts of green and blue spaces: vegetation covers ~34% (forests, parks, agriculture) plus ~7% surface waters (SenUVK, 2019a).

Our study site is located at the grounds of the Leibniz-Institute of Freshwater Ecology and Inland Fisheries (IGB), roughly 220 m north of Lake Müggelsee (Berlin's largest lake) (Figure 1b). The geology is characterized by sand and gravel deposits of the Berlin-Warsaw glacial spillway, (Geological Atlas Berlin, 2007 SenUVK online). The surrounding district (Figure 1b) is characterized by residential areas and roads (38%), forest (40%), water bodies (12%) and public green space (0.06%; SenUVK, 2019b). The study site is a park-like space with older trees (~30–100 years old) surrounded by brick buildings of former 19th-century water works and extensive rough grassland above subsurface slow sand filter systems, which were used for drinking water treatment until the beginning of the 1990s (SenUVK, 2018, online). Within a 100 m radius of the study site center (Figure 1c), premises are covered by buildings (10%), different types of non-irrigated urban green spaces, including grassland (49%), shrubs (8%) and trees (17%); and streets, semi-permeable or sealed pathways and parking spaces (16%).

The experiment focused on two small areas: one tree dominated, the other grassland dominated and both ~16 m apart (Figure 1c). The grassland site was covered by grass (e.g., *Lolium perenne*,

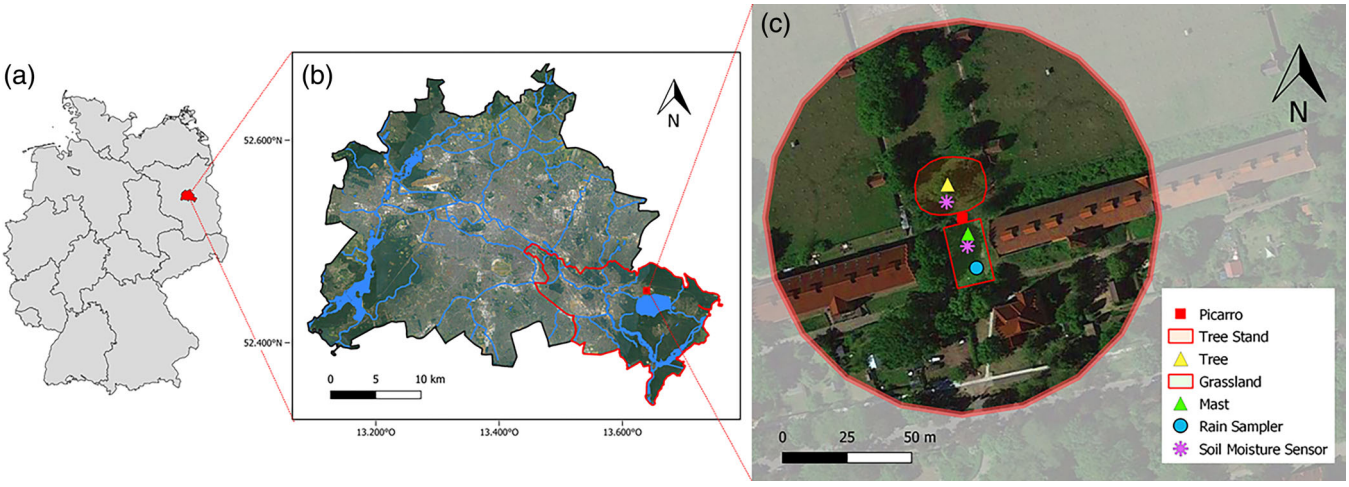

FIGURE 1 Location of Berlin within Germany and map of Berlin (a, b); and the study site at IGB Berlin (c) with the two sampling sites (75 m radius from centre) grassland with flagmast and tree site with Acer platanoides; and installations of atmospheric water vapour in situ measurements, sap flow and soil moisture measurements and precipitation sampler. *Source*: Basemap: Google Satellite.

Arrhenatherum elatius) and herbs (e.g., *Trifolium pratense, Achillea millefolium*) of 30–50 cm in height. It was mowed twice a year and can be referred to as an urban meadow (Norton et al., 2019). The tree site was dominated by black locust, lime, oak, birch and maple trees. We selected one dominant maple tree (*Acer platanoides*) with a stem diameter of 550 mm (measured in August 2021) and height of ~16 m. In other studies, *Acer platanoides* has been shown to have a high drought tolerance (Kunz et al., 2016) and that it can maintain low leaf gas exchange rates (Gillner et al., 2015).

The soils reflect anthropogenic impacts, such as partly backfilled ground after construction work. They are classified as Anthrosols (SenUVK, Aey et al., 2017, online), which consist of debris, sandy materials and a shallow humus layer from extensive gardening.

3 | DATA AND METHODS

3.1 | Monitoring

The study period focused on 20 August to 3 November 2021 (though several variables were measured for longer to provide context of antecedent conditions; see details below). Meteorological data (air temperature, precipitation amount, wind speed and direction, relative humidity, air pressure, global radiation (using a weather station, Thies GmbH)) were available from the rooftop of IGB ~300 m away. Additionally on site, precipitation (via a tipping bucket raingauge, 0.2 mm/tip, precision ±3% of total rainfall; AeroCone® Rain Collector, Davis Instruments, Hayward) was recorded with a CR800 Datalogger (Campbell Scientific, Inc. Logan) logging every 15 min. Temperature was recorded (every 5 min) with BetaTherm 100K6A1IA Thermistors T107 (Campbell Scientific, Inc. Logan; tolerance ±0.2°C (over 0°–50°C)], with a CR300 Datalogger (Campbell Scientific, Inc. Logan). Precipitation and temperature data were verified against data from the German Weather Service (DWD) of the 'Berlin-Marzahn' station (DWD, 2023a) (Station ID: 420), ~12 km north of the study site.

Precipitation for stable water isotope analysis was collected using a HDPE deposition sampler (100 cm^2 opening; Umwelt-Geräte-Technik GmbH, Müncheberg, Germany). Overall, 32 daily and 15 bulk (interval ~ weekly) samples with precipitation >1 mm (to minimize evaporation effects) were collected between July and November 2021. Further, daily precipitation samples were collected ~350 m away from the study site with an autosampler (ISCO 3700, Teledyne Isco, Lincoln) at a 24 h interval. All autosampler bottles were filled with a paraffin layer of >0.5 cm in thickness (after IAEA/GNIP, 2014) to avoid evaporative effects. Additionally, groundwater samples were taken weekly with a submersible pump (COMET-Pumpen Systemtechnik GmbH & Co. KG, Pfaffschwende, Germany) from a well on the IGB grounds ~300 m away from the site.

For isotope analysis of the liquid water samples at the IGB laboratory, samples were filtered (0.2 µm cellulose acetate) and decanted into 1.5 mL glass vials (LLG LABWARE). They were analysed by cavity ring-down spectroscopy (CRDS) with a L2130-i Isotopic Water Analyser (PICARRO, INC., Santa Clara, CA) using four standards for a linear correction function and which were referenced against three primary standards of the International Atomic Energy Agency (IAEA) for calibration [VSMOW2 (Vienna Standard Mean Ocean Water 2), GRESP (Greenland Summit Precipitation) and SLAP2 (Standard Light Antarctic Precipitation 2)]. Liquid samples were injected six times and the first three injections discarded. To screen for interference from organics, the ChemCorrect software (Picarro, Inc.) was applied and contaminated samples were discarded. After quality-checking and averaging multiple analyses for each sample, the results were expressed in δ-notation with Vienna Standard Mean Ocean Water (VSMOW). Analytical precision was 0.05‰ standard deviation (SD) for $\delta^{18}O$ and 0.14‰ SD for δD.

Stable isotopes of atmospheric water vapour (δ_v) were measured in situ at the tree-dominated and grassland sites, respectively at 0.15, 2 and 10 m height to capture the effects of vegetation heterogeneity and potential turbulence within an urban surface boundary layer. To monitor the elevation profile above the grassland, a 10 m flag mast with ~100 cm long perpendicular poles at the required sample points was set up (Figure 2). At the tree site, we measured directly at the trunk within the canopy of the maple tree. Due to logistical reasons, the measurement campaign could start on 20 August 2021 above the grassland and on 03.09.2021 at the tree site.

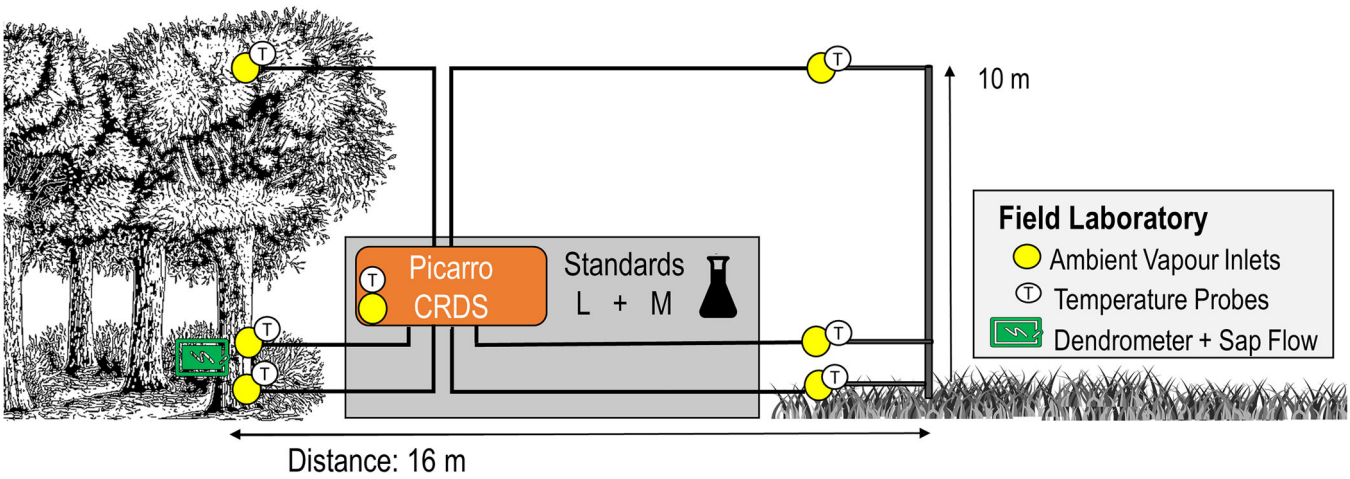

FIGURE 2 Conceptual diagram of the general in situ isotope measuring setup. Ambient vapour inlets, which were installed at the tree, at the mast above grassland and in the CRDS box are shown as yellow dots with corresponding temperature probes marked as 'T'.

We performed in situ real-time sequential measurements of water vapour via CRDS (Picarro L2130-i, Picarro Inc., Santa Clara, CA) placed in a box between the sampling sites. Air inlets and CRDS were connected with polytetrafluoroethylene (PTFE) tubing (1.6 mm x 3.2 mm). We used PET bottles covered with aluminium foil to prevent the inlets from rain and sun exposure. Each tube inlet (Figure 2) was sampled for 20 min in resolution of seconds. Then sampling was switched automatically to the next one; resulting in a 2-hourly resolution for each inlet. Such sequential monitoring of stable water isotopes is a common technique for longer-term (over several weeks) measurements that include different inlet locations to collect powerful data sets using one CRDS (cf. Rothfuss et al., 2015; Steen-Larsen et al., 2013). We only used the data when a measurement showed stable values (i.e., ranges of 2‰ for ^{2}H and 0.3‰ for ^{18}O). In addition, the first 5 min of data after switching inlets were always discarded to avoid memory effects. Prior the vapour entering the CRDS unit, a preceding sub-micron particulate filter was connected to prevent liquid water from entering by creating a low dew point by lowering the air pressure. The sample flow rate was at 0.04 L/min. Water vapour concentrations were always above 6000 ppm (this is where the concentration-dependent deviation becomes low and thus measurement precision is not compromised).

To allow for later conversion of δ_v measurements into liquid water isotope values, temperature probes were installed at all heights near the tube inlets at both sites with BetaTherm 100K6A1IA Thermistors T107 (Campbell Scientific, Inc. Logan; tolerance ±0.2°C (over 0°–50°C)], with a CR300 Datalogger (Campbell Scientific, Inc. Logan) logging mean values every 5 min from second-resoluted data.

Condensation can be a significant issue during in situ measurements (Beyer et al., 2020). To avoid tube condensation resulting from temperature differences, heating cables (ILLw.CT/Qx, Quintex GmbH, Lauda-Königshofen, Germany) were installed and wrapped with the tube in insulation material (cf. Gaj et al., 2016). The cables were controlled via an automatic multi-socket (Gembird 235 EG-PMS2, Gembird Software Ltd., Almere, The Netherlands) to prevent overheating in summer. The PTFE-tubes were flushed weekly with dry air or when condensation was detected for 10 min per probe to remove any water (Beyer et al., 2020). To minimize condensation effects, the measurements were checked daily. Condensation was detected via unstable measurement sequences, when there was no stable plateau of water concentration [ppm] and isotope ratios. In addition, we also checked for condensation at the multiport valve which would be reflected in high and stable water concentrations and sudden drops after the sequence starts together with a gradual rise of isotopic signatures and a sudden drop when the water bubble runs through the tube. Data were discarded when condensation inside the system was identified in the respective tube until normal measurements, that is, without signs of condensations, have been established. Relative humidity at the tube inlets was calculated from water concentration (ppm), temperature and atmospheric pressure with the 'R'-Package 'humidity' (Cai, 2019).

By combining δ_v and temperature data from each inlet, we derived the values for all heights of temperature-dependent equilibrium fractionation from vapour to liquid (i.e., vapour-liquid equilibrated values) with the correction formulated by Majoube (1971):

$$\alpha = exp\frac{a\left(\frac{10^6}{T_k^2}\right)+b\left(\frac{10^3}{T_k}\right)+c}{1000}, \quad (1)$$

where α is the isotopic fractionation factor, T_k is the temperature (in K), and a, b, and c are empirical parameters that vary depending on the isotopologue. All values of isotopic compositions are given in liquid phase and relative to Vienna Standard Mean Ocean Water (VSMOW).

To investigate the local evaporative effects, the line-conditioned excess (short lc-excess) (see Landwehr & Coplen, 2006) was calculated. The lc-excess describes the deviation of the sample from the local meteoric water line (LMWL):

$$lc-excess = \delta^2H - a\cdot\delta^{18}O - b, \quad (2)$$

where a is the slope and b is the intercept of the weighted isotopic composition of the local precipitation. The LMWL was calculated by amount-weighted least square regression (Hughes & Crawford, 2012) from daily precipitation isotopes measured at IGB from July until November 2021.

In order to ensure stable and reliable values to offset variability in the field, the stability of the CRDS was tested in the lab before installing the setup outside. In addition, during the sampling campaign, we calibrated once a week (cf. calibration periods Steen-Larsen et al., 2013) with two standards. Stored in sealed glass containers, the standards were connected to the CRDS for two-point calibrations via linear regression of the δ_v measurements (liquid values: light: ^{2}H −109.91‰/^{18}O −17.86‰; medium: ^{2}H −56.7‰/^{18}O −7.68‰). To account for times between calibrations, we linearly interpolated the functions between calibration dates.

We also monitored sap velocities and stem circumference of the maple tree to gain further insights into the ecohydrological dynamics of the tree (e.g., transpiration patterns, stem growth). Two sap flow sensors (SFM-4, Umwelt-Geräte-Technik GmbH, Müncheberg, Germany; ±0.1 cm/h heat velocity precision) were installed at breast height (1.3 m) at the north and south side of the tree stem. The sap flow sensors work according to the heat ratio method by Marshall (1958). Potential evapotranspiration (PET) was estimated using the FAO Penman–Monteith method (Allen, 1998) with 'R'-Package 'Evapotranspiration' (Guo, 2022). To investigate dynamics during the growing season, both daily and hourly mean sap velocity (cm/h) and PET were then normalized (to $sapvelocity_{norm}$ and PET_{norm}, respectively) by feature scaling; this allowed identification of periods where sapflow was reduced relative to atmospheric demand. One dendrometer [DR Radius Dendrometer, Ecomatik, Dachau, Ger170; accuracy max. ± 4.5% of the measured value (stable offset)] was also installed to measure stem diameter dynamics [mm] at high temporal resolution to identify tree growth as well as swelling/ shrinking patterns. Sap velocity and stem increments were logged as 15 min intervals using a

CR300 Datalogger (Campbell Scientific, Inc. Logan). To get insights into the moisture dynamics underneath canopy, throughfall amount was also sampled manually at a height of 30 cm above ground using four rain gauges (Rain gauge kit, S. Brannan & Sons, Cleator Moor, UK) which were installed 1 and 3 m, respectively, north and south of the tree's stem.

Volumetric soil water content and soil temperature were measured at both sites (Figure 2) by soil moisture temperature probes (SMT-100, Umwelt-Geräte-Technik GmbH, Müncheberg, Germany) in the upper soil at 6 cm depth. Recording took place with a CR800 Datalogger (Campbell Scientific, Inc. Logan) with a 15 min frequency and a precision of ±3% for volumetric soil water content and ± 0.2°C for soil temperature. Groundwater level in one well was monitored with an automatic datalogger (groundwater level probe) at an interval of 15 min (see location in Figure 1c).

3.2 | Testing differences, correlations and the equilibrium assumption

In order to analyse differences and correlations between the different data sets to understand ecohydrological interactions, we performed several statistical tests. Each data set was tested for normality using Shapiro–Wilk (Shapiro & Wilk, 1965). If normally distributed, we performed simple *t*-statistics (Student, 1908) to test for significant differences. If data were skewed or non-normal, we performed non-parametric alternatives: Wilcoxon signed-rank test for two groups (Wilcoxon, 1945) and Kruskal-Wallis test by ranks for more than two groups (Kruskal & Wallis, 1952). To test correlations of non-linear data we applied Spearman's rho statistic (Spearman, 1904).

Due to the nature of the high-resolution data set of δ_v, we could also test the equilibrium assumption of δ_v and δ precipitation for the sampling period using the following equation:

$$\Delta R_{atm} = R_v - R_p, \tag{3}$$

where R_v and R_p are the liquid Majoube-corrected isotope ratios of δ_v and liquid isotope ratios of precipitation and ΔR_{atm} is the difference in isotope ratios of water vapour and precipitation in atmosphere. If $\Delta R_{atm} = 0$, a perfect equilibrium between precipitation and δ_v isotope ratios prevails. We used the daily means of δ precipitation and of δ_v at 2 m height for the tree site and grassland site separately to compare both types of landcover. ΔR_{atm} was calculated for days when precipitation occurred.

4 | RESULTS

4.1 | Hydrometeorological conditions

Figure 3 shows the variability in hydrometeorological variables during the study period (20 August–03 November 2021) in the context of a longer 5-month period. Preceding conditions in July were hot with mean temperatures of 21.4°C and with high precipitation amounts

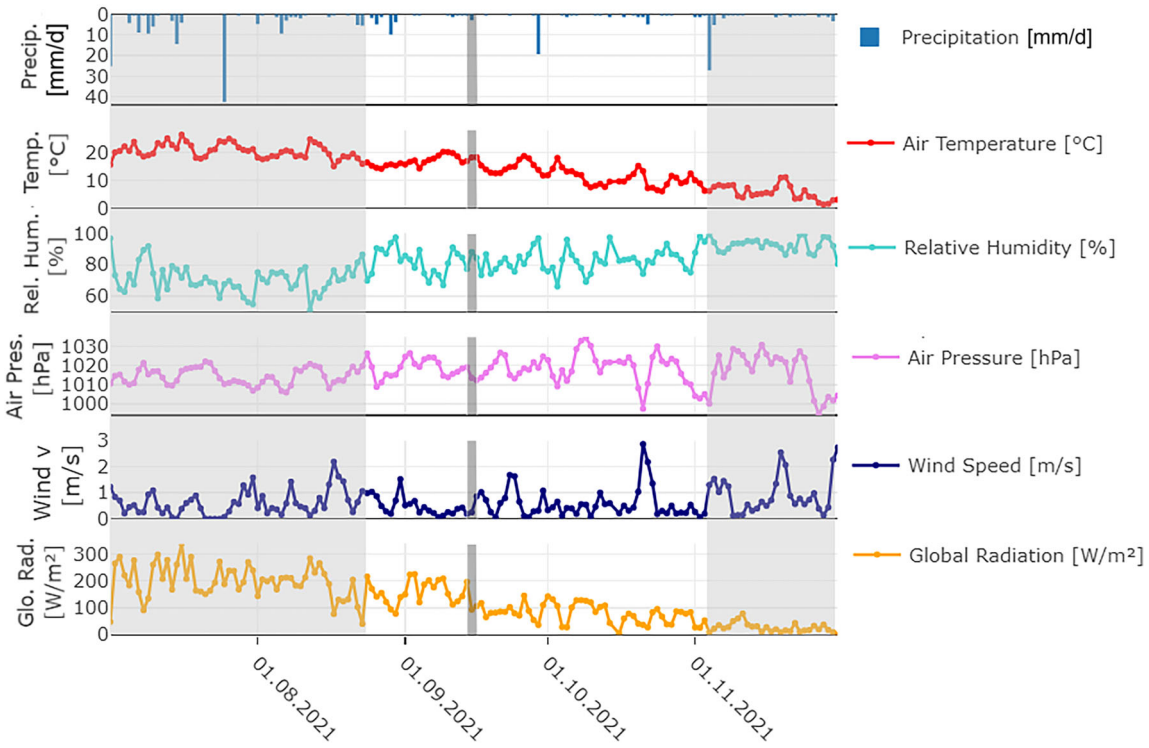

FIGURE 3 Time series of daily hydroclimate data during the study period (July–November 2021) [precipitation (mm), air temperature (°C), relative humidity (%), windspeed (m/s), global radiation (W/m^2)] with the periods before and after the CRDS measurements shaded in grey and the one in detail investigated event marked with the grey bar (see also Figure 7).

(120 mm) exceeding the long-term average for July in Berlin-Marzahn [19.9°C, 75.3 mm; (DWD, 2023b)], including a large storm event in July (> 40 mm in 1 h on 25 July). During the study period, precipitation amounts at the study site (72.6 mm) showed drier conditions compared to the seasonal average in Berlin-Marzahn [147 mm; long-term precipitation August–October (DWD, 2023b)]. Mean air temperature during the study period (14.8°C) reflected radiation and was similar to the long-term seasonal average (August–October). Relative humidity was lower in summer, when temperatures were highest, and increased in autumn. Wind speeds were low (<1 m/s) through most of the sampling, (max value 4.75 m/s on 21 October).

4.2 | Ecohydrological dynamics

Throughfall >1 mm only occurred during three major precipitation events and varied between the sampling points underneath the canopy as follows: 2.8–5.5 mm on 15 September (cf. Figure 7), 9–15 mm on 29 September and 2.5–4.8 mm on 22.10 (events marked in Figure 4). Soil moisture in the sandy upper soils rapidly responded to rainfall at both sites, though any rain signal after the events was quickly lost until more persistent rewetting towards November (Figure 4b). The tree site soil was more responsive to wetting following the heavy rainfall on 29 September (14.4 mm in 1 h). Autumn rewetting was steady from end of September until November. The average groundwater level (Figure 4b) was ~2.3 m b.g.l. and very stable, varying only by 2 cm as it was primarily controlled by the water levels in the lake.

Stem size growth during the study period was insignificantly small (0.2 mm), which is typical for the end of the growing season. Still, swelling of the stem during rainfall and shrinking in the days after events could be detected (Figure 4c). Daily mean sap velocity ranged from 0 to 9.2 cm/h (0–0.92 m/h; Figure 4c,d). The north and south side of the stem showed similar dynamics in sap velocity. Sap velocity signals dropped during rainfall events because of declining atmospheric moisture demand. Normalized for mean sap velocity, sapvelocity$_{norm}$ mostly showed the same ranges as mean ET$_{norm}$ (i.e., also normalized against the mean). During some periods in September, sapvelocity$_{norm}$ exceeded ET$_{norm}$ implying there was a limit on the

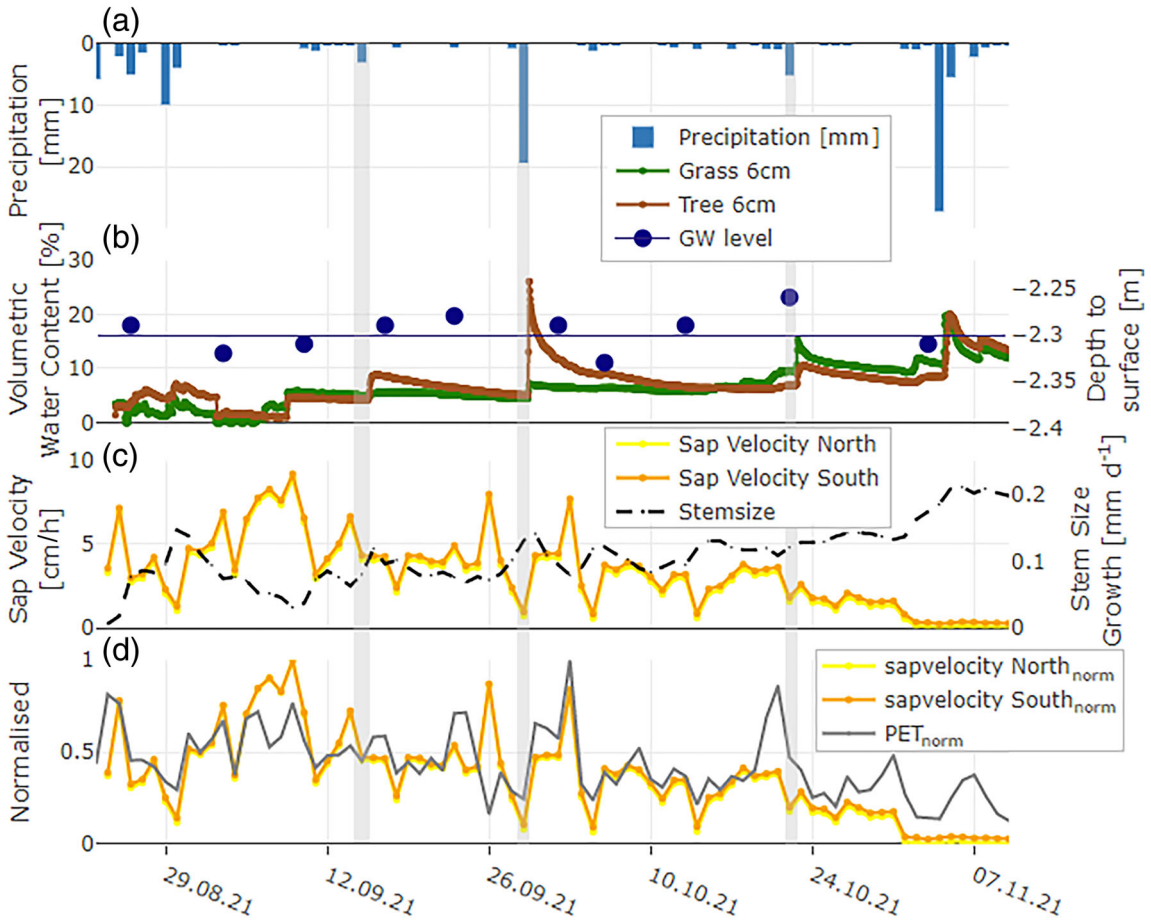

FIGURE 4 Ecohydrological dynamics during the study period: (a) Daily precipitation (mm) (three major throughfall events (on 15 September, 29 September and 22 October) marked in grey bars). (b) Soil moisture [VWC (% h^{-1})] under both land uses and groundwater levels (measured every 2 weeks with horizontal line marking average level). (c) Daily mean sap velocities measured at the maple tree and daily stem size variation as cumulative increments (measured for the stem-radius). (d) Daily normalized sap velocity (sapvelocity$_{norm}$) of the maple tree (North and South facing side of stem) and normalized PET (PET$_{norm}$).

trees meeting atmospheric moisture demand. As the leaf senescence and fall progressed in the middle of October, ET_{norm} exceeded $sapvelocity_{norm}$.

4.3 | Stable water isotope dynamics

Figure 5 shows that stable water isotopes in precipitation were highly variable and more negative (i.e., higher depletion in heavier isotopes) for events in late August and early November. δ_v at the tree and grassland sites (both shown as examples for 2 m height) was often influenced in varying magnitude by rainfall inputs depleted in heavy isotopes. For example, δ_v at the grassland sites (prior to tree monitoring commencing) showed particularly high depletion in heavy isotopes in response to depleted rainfall values at the beginning of September (Figure 5a). Summary statistics of measured stable water isotope values and ranges of precipitation, groundwater and atmospheric vapour δ_v (liquid values) are given in Table 1.

The amount-weighted LMWL of the sampling period (July–November 2021) (Figure 6) was $\delta^2H = 7.71 \pm 0.11 * \delta^{18}O + 7.42$

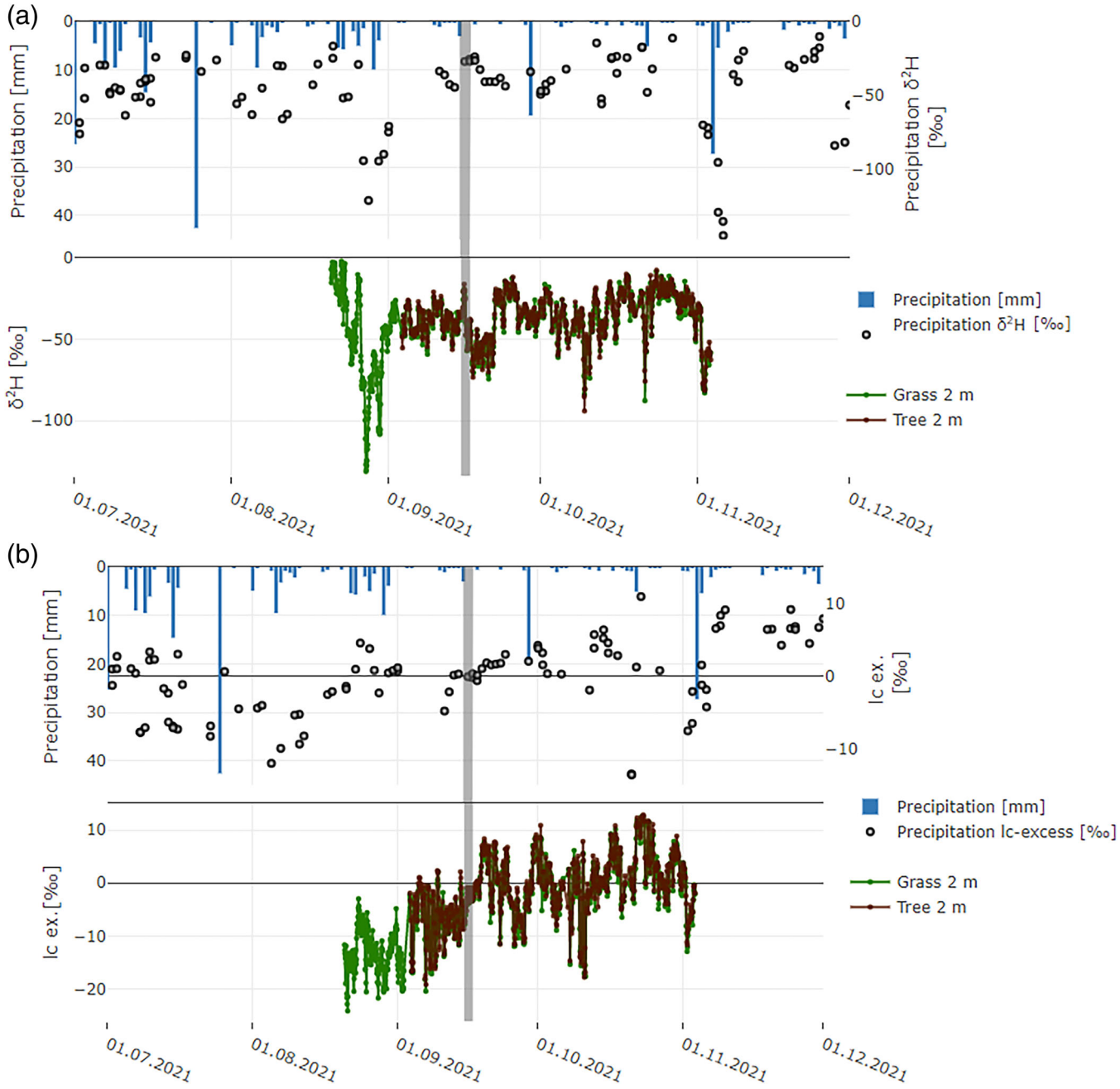

FIGURE 5 Daily precipitation amount, daily stable water isotope ratios of precipitation and hourly δ_v of the grassland and tree site (both shown here for 2 m height, monitoring started 20 August and 3 September for the grassland and tree site, respectively) for (a) δ^2H_v and (b) lc-excess of δ_v (the precipitation event from Figure 7 is marked with grey line).

TABLE 1 Summary statistics of measured stable water isotope values of precipitation, groundwater and atmospheric vapour δ_v (δ values in liquid phase).

	‰	Min	Mean	Max	Median	SD
Precipitation	δ^2H	−145.22	−46.13	−10.161	−40.8	26.27
	$\delta^{18}O$	−19.25	−6.94	−1.44	−6.2	3.39
	lc-excess	−13.6	−0.06	10.93	0.67	5.16
Groundwater	δ^2H	−55.83	−51.17	−47.99	−49.8	2.91
	$\delta^{18}O$	−7.63	−6.68	−5.94	−6.44	0.59
	lc-excess	−9.58	−7.05	−4.41	−7.6	1.66
Vapour						
Grass 0.15 m	δ^2H	−163.91	−116.39	−87.17	−32.53	12.75
	$\delta^{18}O$	−21.01	−15.35	−11.43	−4.81	1.68
	lc-excess	−23.36	−5.49	8.38	−5.07	5.87
Grass 2 m	δ^2H	−165.96	−119.82	−94.9	−35.6	13.23
	$\delta^{18}O$	−22.3	−15.88	−12.06	−5.22	1.85
	lc-excess	−25.16	−4.84	7.32	−4.53	5.92
Grass 10 m	δ^2H	−169.92	−120.52	−85.61	−36.13	13.73
	$\delta^{18}O$	−22.59	−16.05	−12.1	−5.38	1.88
	lc-excess	−20.93	−4.19	8.58	−4.11	5.33
Tree 0.15 m	δ^2H	−164.3	−119.43	−92.33	−34.97	12.65
	$\delta^{18}O$	−22.25	−15.83	−11.88	−5.15	1.81
	lc-excess	−23.42	−4.78	10.9	−4.58	6.12
Tree 2 m	δ^2H	−169.91	−120.14	−92.83	−35.7	13.14
	$\delta^{18}O$	−23.56	−15.94	−12.01	−5.25	1.87
	lc-excess	−24.63	−4.65	9.56	−4.34	6.07
Tree 10 m	δ^2H	−170.32	−120.38	−89.67	−36.26	13.59
	$\delta^{18}O$	−23.48	−16.04	−11.84	−5.41	1.9
	lc-excess	−24.21	−4.15	8.7	−4.03	5.7

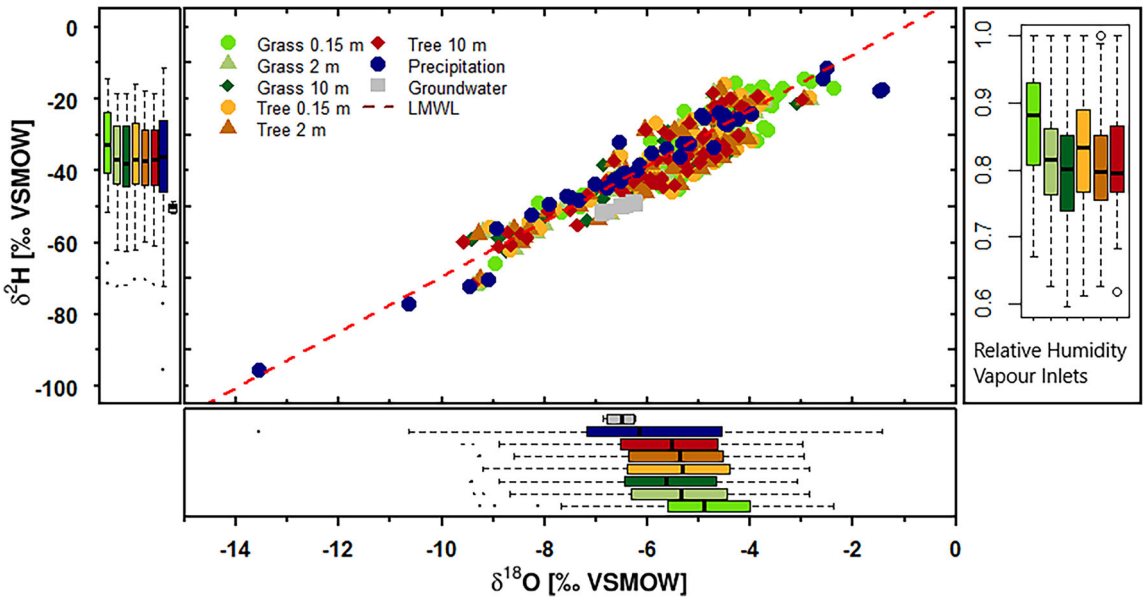

FIGURE 6 Dual isotope plot of δ_v (shown as daily mean) for the three different heights and two vegetation types as well as precipitation (daily) and groundwater (weekly) samples; including relative humidity for the different heights calculated from water concentrations in the vapour tube inlets. Data shown here were sampled between 4 September and 3 November 2021, when sampling was active on both sites. Boxplots show the sample distribution of the data sets.

± 1.12 ($R^2 = 0.987$). lc-excess in precipitation increased from late summer to late autumn, though variability remained high especially in October (Figure 5b). The lc-excess was generally negative at both sites until mid-September, reflecting high energy for evaporation. From Mid-September until November, lc-excess of δ_v was generally positive but more variable. Spearman rank correlation coefficients between precipitation and δ_v of grassland were 0.55 for δ^2H and 0.43 for lc-excess indicating positive correlations for the full study period from 20 August–3 November 2021.

The dual isotope plot (Figure 6) clearly shows that precipitation isotopes were characterized by large ranges (δ^2H −145.2‰ to −10.2‰; $\delta^{18}O$ −19.3‰ to −1.5‰). Groundwater in comparison showed little variation with mean isotopic signatures (Table 1). Beneath the tree canopy, δ_v was more homogenous across the elevation profile than above grass. Grassland showed a higher variance of δ_v within the elevation profile, with a tendency of near-surface air (0.15 m height) to be more enriched in heavy isotopes in comparison to the tree-site, but attenuating with height (Table 1). Overall, the boxplots and median values of grassland δ_v showed a slightly higher range compared to the tree site (Figure 6, Table 1). The Kruskal-Wallis-Test showed significant differences of δ_v (p-values <0.05) between ground-level (0.15 m) and higher elevations (2 m, 10 m) at the grassland, while there were no significant differences (p-values >0.05) between different heights underneath the tree canopy and also no significant differences between both sites at 2 and 10 m. However, the Wilcoxon signed-rank test indicated a p-value of 0.0507 ($\alpha = 0.05$) between the sites for 0.15 m height showing they were significantly different. To assess the relationship between δ_v and corresponding relative humidity at the elevation profiles, we show relative humidity distributions of the vapour inlets in Figure 6. Humidity rates were highest above surface at both sites with a decline with height for grassland. At the tree site relative humidity was higher in the canopy at 10 m height than beneath canopy at 2 m.

We also tested for relationships between δ_v and soil moisture in order to further assess surface evaporation dynamics during the whole study period. After testing Spearman's rank correlation between δ_v for different heights and soil moisture at both sites, only the grassland site indicated a significant positive correlation of soil moisture with δ^2H_v (0.3 at 0.15 m; 0.24 at 2 m; 0.22 at 10 m), but

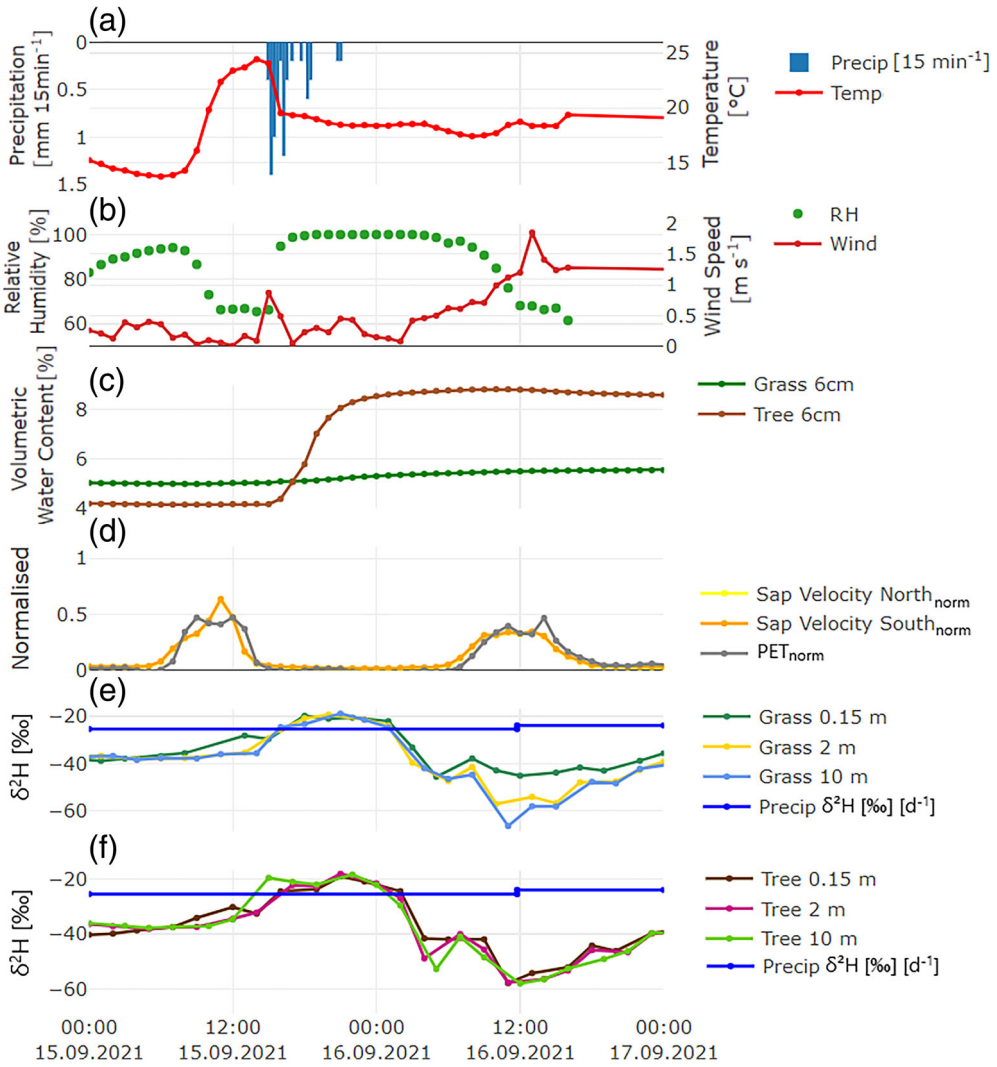

FIGURE 7 Responses of the hourly grassland and tree stand δ^2H_v (e, f) and daily precipitation δ^2H displayed in blue horizontal lines during the precipitation event on 15 September 2021 with 15-min data of (a) precipitation (mm) and temperature (°C), (b) relative humidity (%) and wind speed (m/s), (c) soil moisture as volumetric water content (%), (d) normalized data of sap velocity of maple tree (north and south side of the stem) and PET.

none for $\delta^{18}O_v$. The tree site showed no significant correlations between δ_v and soil moisture for either isotope.

We also investigated higher resolution dynamics of δ_v during different precipitation events, and we display here the event on the afternoon of 15 September 2021 (where 6.6 mm fell between 15:00–18:30; and 2.8–5.5 mm of throughfall occurred) (Figure 7). Both sites showed high δ_v values at night corresponding to the signature of precipitation, with uniform distribution at different heights. The next day, δ_v above grassland reflected clear evaporative losses by enrichment in heavy isotopes just above the surface, when PET and windspeed were higher (Figure 7b,d), which was also observed during the other events (cf. Figures S1, S2). In the tree canopy, no differences of δ_v with height occurred even with increasing sap velocity. During the event, soil water content of the grassland was 4.2% and increased to 5.6% 24 h after the rainfall; whereas soil underneath tree canopy showed greater response to rainfall increasing from 5.0% to 8.7% (Figure 7c).

4.4 | Equilibrium between vapour and precipitation

The difference in isotope ratios of δ_v and precipitation in the atmosphere, ΔR_{atm}, generally deviated from zero (i.e., the equilibrium) at both sites, with higher deviation from the equilibrium between mid-August and mid-September (Figure 8). Responses of ΔR_{atm} after precipitation events showed heterogenous patterns, reflecting varying deviations from equilibrium throughout the monitoring period. In August, grassland showed mostly positive ΔR_{atm}, but also higher deviations of the daily mean, depicting higher values of δ_v compared to precipitation and variations in summer when radiation is high. On an event basis, grassland and tree sites differed slightly in ΔR_{atm} and the timeseries of ΔR_{atm} for $\delta^{18}O$ and δ^2H showed similar patterns.

Boxplots showed higher ΔR_{atm} values at the grassland site (though note that grassland included more data, Figure 9). T-tests did not show significant differences between grassland and tree site for ΔR_{atm} δ^2H ($p = 0.055$) but showed significance for ΔR_{atm} $\delta^{18}O$ ($p = 0.012$), again showing a difference between the two vegetation types in their variation from equilibrium. Median ΔR_{atm} values of δ^2H were 2.95‰

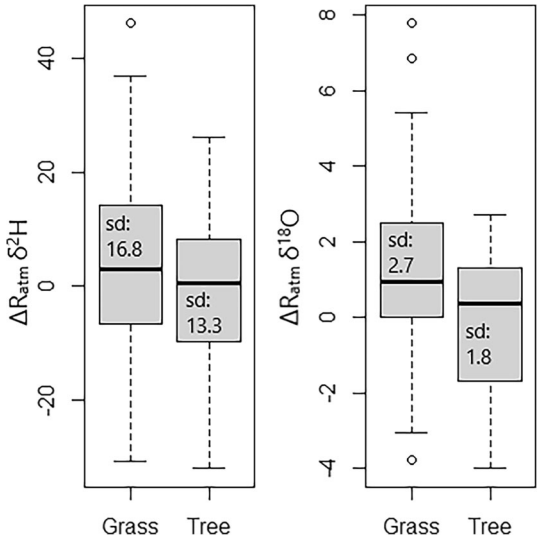

FIGURE 9 ΔR_{atm} distributions of $\delta^{18}O$ and δ^2H of the grassland and tree site exemplary at 2 m height during the whole sampling period.

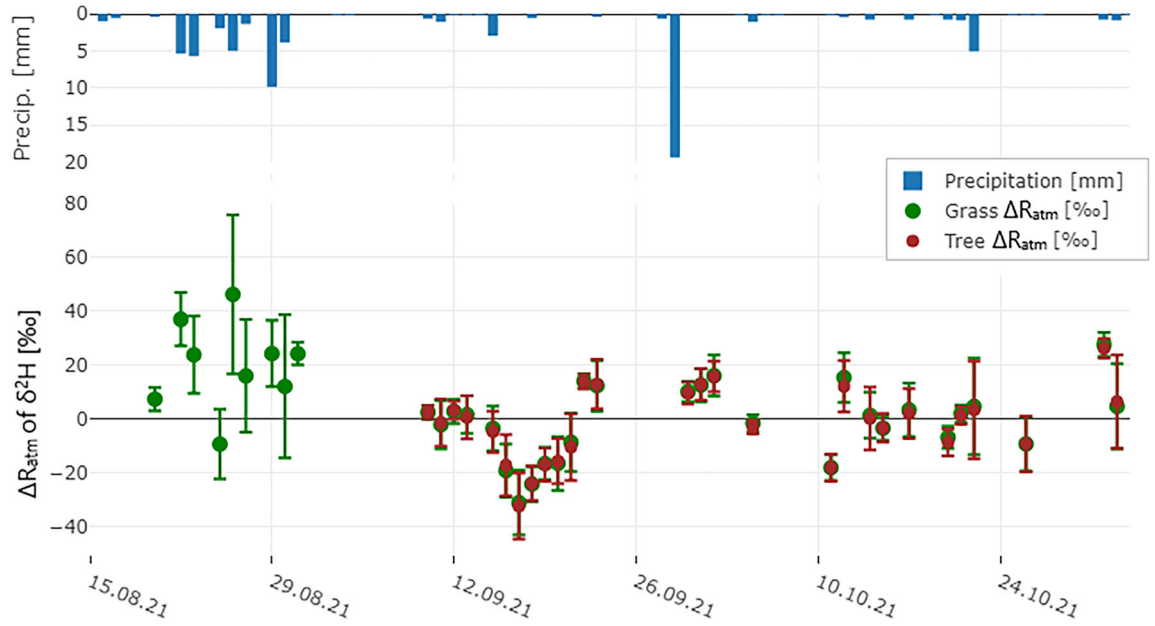

FIGURE 8 Daily rain event ΔR_{atm} of δ^2H exemplary shown at 2 m height for grassland (green; monitoring start 20 August) and tree site (brown; monitoring start 3 September) and daily precipitation amount. Error bars indicating standard deviation of daily mean of δ^2H_v.

and 0.51‰ for $\delta^{18}O$ at the grassland, and 0.51‰ for $\delta^{2}H$ and 0.36‰ for $\delta^{18}O$ at the tree site. Maximum and minimum ΔR_{atm} values at the grassland ranged between −30 and 46‰ and between −3.7 and 7.7‰ for $\delta^{2}H$ and $\delta^{18}O$, respectively. At the tree site they varied between −31 and 26‰ and − 4 and 2.7‰ for $\delta^{2}H$ and $\delta^{18}O$, respectively. Thus, the deviation from equilibrium of δ_v and δ precipitation was greater at the grassland than at the tree stand. The higher and more abundant positive values of ΔR_{atm} at grassland reflect a higher isotopic enrichment of δ_v.

5 | DISCUSSION

5.1 | Vapour stable water isotopes in different urban vegetation

This study showed that a relatively extended (i.e., >2 months) period of continuous sequential in situ monitoring of δ_v could produce novel continuous timeseries for urban green space environments in Berlin. Our distributed network of inlet ports sampling the atmospheric boundary at different heights above contrasting urban green space vegetation produced reliable high-resolution data with a 2-h resolution for each inlet. However, there is no doubt that the method is very labour intensive and requires almost daily maintenance including checking the correct operation of the CRDS, ventilation systems and pumps. Detailed, biweekly data checks of the different inlets are also necessary to detect condensation in the tubes or other unwanted memory effects in the CRDS. In particular, the in situ setup requires a secured environment for the CRDS and vapour tubing (e.g., a locked and fenced box and securing pipes adapted to the study site). Overall, however, we found that in situ monitoring of δ_v needs less regular maintenance than in situ soil water monitoring due to greater condensation issues from temperature contrasts in the deep soil compared to atmospheric vapour (cf. Landgraf et al., 2022).

Monitored δ_v data fluctuated around the LMWL (Figure 6) in equal distribution over the entire study period indicating no dominant influence of non-equilibrium fractionation (Dansgaard, 1964), but disequilibrium occurred at shorter time scales. We found a limited difference between the two vegetation covers reflecting a generally well-mixed boundary. δ_v of grassland showed a slightly higher temporal variability and also higher variance along the height profile compared to the tree site. The only significant difference was that the surface air (at 0.15 m height) above the grassland was more enriched in heavy isotopes, though this was rapidly attenuated with height, corresponding with the humidity elevation profiles at the vapour inlets. This indicates tendencies of grassland and tree canopy to lose or store moisture, respectively, which explains the homogenous profile of δ_v at the tree from lower moisture losses. An in situ study by Griffis et al. (2016) found similar effects of surface evaporation enriching surface boundary layer water vapour and atmospheric loss of light vapour fraction above grassland through the underlying process of kinetic fractionation during evaporation (Craig & Gordon, 1965), while tree canopy protects from such loss.

At the event scale, δ_v showed clear isotopic responses after rain. The response timing was dependent on the time of day being more marked around noon when radiation input is elevated. This is due to the fact that δ_v at hourly timescale is controlled by airmass advection which increases with higher solar radiation (Lee et al., 2006). At the seasonal scale, lc-excess was low in summer and higher in autumn reflecting higher ET in warmer months. A common aspect for all the precipitation events was a close link between the signatures of precipitation and δ_v resulting in positive correlations (0.55 for $\delta^{2}H$ and 0.43 for lc-excess) indicating the influence of rainout and rain-vapour exchange (Bowen et al., 2019). The seasonal amplitude of δ_v can been explained by vertical mixing across the top of the planetary boundary layer (Angert et al., 2008) and Rayleigh processes that are strongly modulated by evaporation and entrainment (Griffis et al., 2016), that is, inflow of an air parcel to another. This shows the importance on testing the assumption of equilibrium between vapour and precipitation.

5.2 | Insights into high-resolution urban ecohydrology

Our results indicated that the urban grassland surface is contributing to the atmospheric moisture affecting water partitioning with the main drivers being high surface evaporation and possibly high transpiration of the grass, high surface temperatures as well as low atmospheric mixing (Figure 10). The measurements from beneath canopy give useful insights for turbulent mixing parameterization of urban canopy layer vertical transport, but direct transpiration imprint could not be measured underneath the canopy.

Additional insights into the processes controlling isotopic composition of δ_v in an urban green space were leveraged by having simultaneous ecohydrological monitoring, that is, measurements of soil moisture, throughfall, sap velocity and tree diameter. At both sites, the overall low soil moisture in the sandy top layer (6 cm depth) increased in response to precipitation events and then decreased rapidly with time reflecting drainage and lateral flow. Grassland showed no response to the major event on 29 September 2021, which is probably due to lateral flows. Soil moisture did only partly respond to smaller events reflecting low infiltration. The low responses to small events indicate evaporative losses from soil and plant interception that contribute—at least in the grass plot—to increased evaporation that affects the isotopic signal at 0.15 m. Further, groundwater levels did not change during the study period indicating that precipitation water was either stored in the soil profile or lost to ET processes. Potential normalized ET_{norm} largely did not exceed total sapvelocity$_{norm}$ of the maple tree during the phase of active leaves indicating the tree was not under drought stress. Additionally, dendrometer data revealed normal stem growth for late summer and autumn reflecting healthy tree vitality, including swelling with precipitation events (cf. Chan et al., 2016). Considering the low top soil moisture and constant sap flux, our results match the findings of Kuhlemann et al. (2021) from another urban green space site in Berlin in that urban tree transpiration rates show a certain resilience to drought (which is of course highly dependent on tree ages and species). Further, the investigated site comprised a group of trees which probably makes a

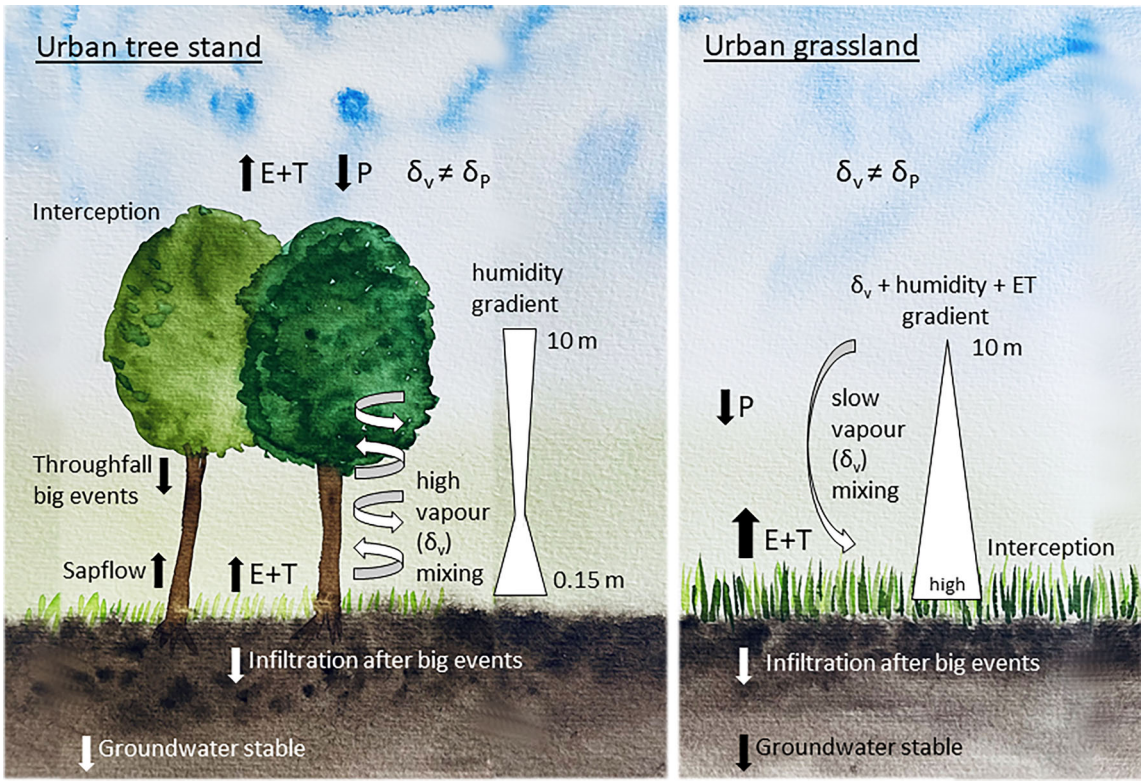

FIGURE 10 Conceptual graphic summarizing the main water and energy fluxes of the two investigated urban green spaces during the monitoring period (20 August–3 November 2021).

difference compared to individual urban trees in another study that showed considerably higher sap flux densities (Ponte et al., 2021).

Interestingly, despite interception evaporation and transpiration from the urban tree canopy after events, there was no imprint on δ_v captured at 10 m compared to lower heights (cf. Berkelhammer et al., 2013). Generally, δ_v variabilities did not correlate with certain measured ecohydrological parameters (e.g., soil moisture) throughout the whole sampling period, which means the isotopic signals from precipitation and boundary layer mixing processes were most influential, though δ_v responded to changes in potential ET during the warmer period until the end of September.

Such insights into high-resolution dynamics of ecohydrological fluxes and partitioning can contribute to improved strategies of urban green space management in the future, for example, via improved parametrization of ecohydrological models to quantify ET fluxes (e.g., Smith et al., 2022). There is great potential for more detailed monitoring of urban canopy ET by more distributed networks in canopies, for example, it would be interesting to measure at least 5 m over an urban canopy or even higher—similar to Braden-Behrens et al. (2019).

5.3 | Testing the assumption of equilibrium between vapour and precipitation

Previous studies (Lekshmy et al., 2018; Penchenat et al., 2020; Vimeux & Risi, 2021) showed that the equilibrium assumption is more robust at subseasonal, longer time scales than for individual rain events. Lee et al. (2006) found that during rain events, vapour in the surface layer developed in general a state of equilibrium with the falling raindrops. In our study, this assumption was not robust at the subseasonal scale and did not confirm an establishment of an equilibrium.

ΔR_{atm} (i.e., difference in isotope ratios of water vapour and precipitation in atmosphere) was greater and showed more positive values in summer reflecting that vapour was more enriched in heavy isotopes than precipitation during summer. Potential reasons for this are (as discussed by Penchenat et al., 2020) that raindrops formed at high elevation (Dansgaard, 1964), precipitation came from convective events with big raindrops or high tree transpiration rates from deeper sources prevented vapour from equilibrium with precipitation. Additionally, high transpiration rates lead to isotopic enrichment of δ_v (Gonfiantini et al., 1965) and could generate higher deviation from δ_v with precipitation.

Testing the equilibrium assumption is especially important for areas with a distinct microclimate like cities as previous studies showed that equilibrium estimates can be biased (Fiorella et al., 2019). Further, different regions of the World show diverging results for ΔR_{atm} depending on climate, altitude and latitude. For example, Mercer et al. (2020) showed that the equilibrium assumption does not hold in continental mountain environments. This underlines the importance of these data, as by going beyond the standard assumption of equilibrium in urban ecohydrology, we could improve simple mixing models, complex process-based, isotope-aided ecohydrological models like EcH$_2$O-iso (Kuppel et al., 2018), estimations in keeling plot

(Keeling, 1958) and the Craig and Gordon (1965) approach (cf. Rothfuss et al., 2021). In particular, in isotope-aided ecohydrological models, this could allow more robust estimates of resolving ET into its E and T components.

6 | CONCLUSION

We monitored stable water isotopes in liquid precipitation and atmospheric water vapour (δ_v) using in situ CRDS over a two-month period in an urban green space area in Berlin, Germany. δ_v was monitored at multiple heights (0.15, 2 and 10 m) in different vegetation: grassland and forest plots. Our distributed sampling network of inlet ports produced novel, reliable and stable high-resolution data with a 2-h resolution for each inlet.

We have shown that the isotopic composition of δ_v above both land uses was highly dynamic and positively correlated with that of rainfall indicating the changing sources of atmospheric moisture. The isotopic composition of δ_v was similar across most heights of the 10 m profiles and between the two plots indicating limited aerodynamic mixing. Only the surface at ~0.15 m height above the grassland showed significant differences in δ_v, with pronounced enrichment in heavy isotopes indicative of evaporative fractionation immediately after rainfall events.

We combined this isotope monitoring with hydroclimatic monitoring and measurements of ecohydrological variables such as sap flow, stem size, soil moisture, throughfall. At both sites, the overall low top soil moisture increased in response to precipitation and then decreased after the events reflecting drainage and evaporative losses, with evaporation being more pronounced at the grassland. During some days in September, normalized PET_{norm} did exceed total $sapvelocity_{norm}$ of the maple tree during the phase of active leaves potentially indicating periods of drought stress on the tree. Dendrometer data revealed normal stem growth for late summer and autumn showing no drought stress. Despite interception evaporation and transpiration from the tree canopy after events, there was no imprint on δ_v captured at 10 m compared to lower heights. Our results indicate occasional dis-equilibrium between water vapour and precipitation isotopes.

Our set up provided novel insights into high-resolution dynamics of water cycling and partitioning in an urban green space. Such data sets can contribute to improved urban planning strategies providing a new evidence-base for vegetation management choices considering urban water cycling. Such data has also the potential to better constrain the isotopic interface between the atmosphere and the land surface. Importantly, it can be incorporated into tracer-aided ecohydrological models that can resolve evapotranspiration fluxes and improve these estimations.

However, more research is needed to upscale these findings to the canopy and city scales. More detailed monitoring of urban canopy ET by more distributed networks in and above canopies will benefit further investigations.

ACKNOWLEDGEMENTS

This study was funded through the German Research Foundation (DFG) as part of the Research Training Group 'Urban Water Interfaces' (UWI; GRK2032/2) and the Einstein Foundation as part of the 'Modelling surface and groundwater with isotopes in urban catchments' (MOSAIC) project. Funding for Dörthe Tetzlaff was also received through the Einstein Research Unit 'Climate and Water under Change' from the Einstein Foundation Berlin and Berlin University Alliance (grant no. ERU-2020-609) and the project BiNatur (BMBF No. 16LW0156). We also acknowledge the BMBF (funding code 033W034A), which supported the stable isotope laboratory and in situ laser analyser. Contributions from Chris Soulsby have also been supported by the Leverhulme Trust through the ISO-LAND project (grant no. RPG 2018 375). We thank all colleagues involved in the ecohydrological monitoring and daily precipitation and groundwater sampling, but in particular are grateful to Jan Christopher, Jonas Freymüller and Jessica Landgraf. Open Access funding enabled and organized by Projekt DEAL.

DATA AVAILABILITY STATEMENT

The data that support the findings of this study are available from the corresponding author upon reasonable request.

ORCID

Ann-Marie Ring https://orcid.org/0009-0001-3445-1622
Maren Dubbert https://orcid.org/0000-0002-2352-8516
Chris Soulsby https://orcid.org/0000-0001-6910-2118

REFERENCES

Aboelnga, H., Ribbe, L., Frechen, F.-B., & Saghir, J. (2019). Urban water security: Definition and assessment framework. *Resources*, *8*(4), 178. https://doi.org/10.3390/resources8040178

Aemisegger, F., Sturm, P., Graf, P., Sodemann, H., Pfahl, S., Knohl, A., & Wernli, H. (2012). Measuring variations of $\delta^{18}O$ and $\delta^{2}H$ in atmospheric water vapour using two commercial laser-based spectrometers: An instrument characterisation study. *Atmospheric Measurement Techniques*, *5*(7), 1491–1511. https://doi.org/10.5194/amt-5-1491-2012

Aey, W., Bíró, P., Claußen, U., Gerstenberg, J., Grenzius, R., & Metzlaff, G. (2017). Bodengesellschaften. https://www.berlin.de/umweltatlas/boden/bodengesellschaften/2015/karten/artikel.919905.php

Ahiablame, L. M., Engel, B. A., & Chaubey, I. (2012). Effectiveness of low impact development practices: Literature review and suggestions for future research. *Water, Air, & Soil Pollution*, *223*(7), 4253–4273. https://doi.org/10.1007/s11270-012-1189-2

Allen, R. G. (1998). Crop evapotranspiration-guideline for computing crop water requirements. *Irrigation and Drainage*, *56*, 300.

Amt für Statistik Berlin-Brandenburg. (2023). *Bevölkerungsstand* 2022. https://www.statistik-berlin-brandenburg.de/bevoelkerung/demografie/bevoelkerungsstand

Angert, A., Lee, J.-E., & Yakir, D. (2008). Seasonal variations in the isotopic composition of near-surface water vapour in the eastern Mediterranean. *Tellus B: Chemical and Physical Meteorology*, *60*(4), 674. https://doi.org/10.1111/j.1600-0889.2008.00357.x

Benettin, P., Volkmann, T. H. M., von Freyberg, J., Frentress, J., Penna, D., Dawson, T. E., & Kirchner, J. W. (2018). Effects of climatic seasonality on the isotopic composition of evaporating soil waters. *Hydrology and*

Earth System Sciences, *22*(5), 2881–2890. https://doi.org/10.5194/hess-22-2881-2018

Berkelhammer, M., Hu, J., Bailey, A., Noone, D. C., Still, C. J., Barnard, H., Gochis, D., Hsiao, G. S., Rahn, T., & Turnipseed, A. (2013). The nocturnal water cycle in an open-canopy forest. *Journal of Geophysical Research: Atmospheres*, *118*(17), 10225–10242. https://doi.org/10.1002/jgrd.50701

Beyer, M., Kühnhammer, K., & Dubbert, M. (2020). In situ measurements of soil and plant water isotopes: A review of approaches, practical considerations and a vision for the future. *Hydrology and Earth System Sciences*, *24*(9), 4413–4440. https://doi.org/10.5194/hess-24-4413-2020

Bichai, F., & Cabrera Flamini, A. (2018). The water-Sensitive City: Implications of an urban water management paradigm and its globalization. *WIREs Water*, *5*(3), e1276. https://doi.org/10.1002/wat2.1276

BMUB. (2018). *White Paper: Green Spaces in the City: Green Spaces in the City – For a more liveable future*. https://www.bmwsb.bund.de/SharedDocs/downloads/Webs/BMWSB/DE/publikationen/wohnen/weissbuch-stadtgruen-en.pdf?__blob=publicationFile&v=3

Bowen, G. J., Cai, Z., Fiorella, R. P., & Putman, A. L. (2019). Isotopes in the water cycle: Regional- to global-scale patterns and applications. *Annual Review of Earth and Planetary Sciences*, *47*(1), 453–479. https://doi.org/10.1146/annurev-earth-053018-060220

Braden-Behrens, J., Markwitz, C., & Knohl, A. (2019). Eddy covariance measurements of the dual-isotope composition of evapotranspiration. *Agricultural and Forest Meteorology*, *269-270*, 203–219. https://doi.org/10.1016/j.agrformet.2019.01.035

Cai, J. (2019). *Humidity*. R package. https://cran.r-project.org/package=humidity

Chan, T., Hölttä, T., Berninger, F., Mäkinen, H., Nöjd, P., Mencuccini, M., & Nikinmaa, E. (2016). Separating water-potential induced swelling and shrinking from measured radial stem variations reveals a cambial growth and osmotic concentration signal. *Plant, Cell & Environment*, *39*(2), 233–244. https://doi.org/10.1111/pce.12541

Coenders-Gerrits, A. M. J., van der Ent, R. J., Bogaard, T. A., Wang-Erlandsson, L., Hrachowitz, M., & Savenije, H. H. G. (2014). Uncertainties in transpiration estimates. *Nature*, *506*(7487), E1–E2. https://doi.org/10.1038/nature12925

Craig, H., & Gordon, L. I. (1965). Deuterium and oxygen 18 variations in the ocean and the marine atmosphere. *Stable Isotopes in Oceanographic Studies and Paleo-Temperatures*, *1965*, 9–130.

Dansgaard, W. (1964). Stable isotopes in precipitation. *Tellus*, *16*(4), 436–468. https://doi.org/10.1111/j.2153-3490.1964.tb00181.x

Dubbert, M., Cuntz, M., Piayda, A., & Werner, C. (2014). Oxygen isotope signatures of transpired water vapor: The role of isotopic non-steady-state transpiration under natural conditions. *The New Phytologist*, *203*(4), 1242–1252. https://doi.org/10.1111/nph.12878

Dubbert, M., & Werner, C. (2018). Water fluxes mediated by vegetation: Emerging isotopic insights at the soil and atmosphere interfaces. *The New Phytologist*, *221*(4), 1754–1763. https://doi.org/10.1111/nph.15547

DWD. (2023a). *Climate Data Center (CDC) of German Weather Service*. https://opendata.dwd.de/climate_environment/CDC/observations_germany/climate/daily/kl/

DWD. (2023b). *Longterm Means*. https://www.dwd.de/DE/leistungen/klimadatendeutschland/vielj_mittelwerte.html

Ehleringer, J. R., Barnette, J. E., Jameel, Y., Tipple, B. J., & Bowen, G. J. (2016). Urban water – a new frontier in isotope hydrology. *Isotopes in Environmental and Health Studies*, *52*(4–5), 477–486. https://doi.org/10.1080/10256016.2016.1171217

Falkenmark, M., & Rockström, J. (2006). The new blue and green water paradigm: Breaking new ground for water resources planning and management. *Journal of Water Resources Planning and Management*, *132*(3), 129–132. https://doi.org/10.1061/(ASCE)0733-9496(2006)132:3(129)

Fiorella, R. P., West, J. B., & Bowen, G. J. (2019). Biased estimates of the isotope ratios of steady-state evaporation from the assumption of equilibrium between vapour and precipitation. *Hydrological Processes*, *33*(19), 2576–2590. https://doi.org/10.1002/hyp.13531

Gaj, M., Beyer, M., Koeniger, P., Wanke, H., Hamutoko, J., & Himmelsbach, T. (2016). In situ unsaturated zone water stable isotope (^{2}H and ^{18}O) measurements in semi-arid environments: A soil water balance. *Hydrology and Earth System Sciences*, *20*(2), 715–731. https://doi.org/10.5194/hess-20-715-2016

Galewsky, J., Steen-Larsen, H. C., Field, R. D., Worden, J., Risi, C., & Schneider, M. (2016). Stable isotopes in atmospheric water vapor and applications to the hydrologic cycle. *Reviews of Geophysics*, *54*(4), 809–865. https://doi.org/10.1002/2015RG000512

Gao, J., Yao, T., Masson-Delmotte, V., Steen-Larsen, H. C., & Wang, W. (2019). Collapsing glaciers threaten Asia's water supplies. *Nature*, *565*(7737), 19–21. https://doi.org/10.1038/d41586-018-07838-4

Gat, J. R. (1996). Oxygen and hydrogen isotopes IN the hydrologic cycle. *Annual Review of Earth and Planetary Sciences*, *24*(1), 225–262. https://doi.org/10.1146/annurev.earth.24.1.225

Gat, J. R. (2000). Atmospheric water balance?The isotopic perspective. *Hydrological Processes*, *14*(8), 1357–1369. https://doi.org/10.1002/1099-1085(20000615)14:8%3C1357::AID-HYP986%3E3.0.CO;2-7

Geological Atlas Berlin. (2007). SenUVK online, Hörmann, Ulrike; Limberg, Alexander; Schröter, Wolfhard. https://www.berlin.de/umweltatlas/boden/geologische-skizze/2007/karten/artikel.964029.php

Gillefalk, M., Tetzlaff, D., Hinkelmann, R., Kuhlemann, L.-M., Smith, A., Meier, F., Maneta, M. P., & Soulsby, C. (2021). Quantifying the effects of urban green space on water partitioning and ages using an isotope-based ecohydrological model. *Hydrology and Earth System Sciences*, *25*(6), 3635–3652. https://doi.org/10.5194/hess-25-3635-2021

Gillner, S., Korn, S., & Roloff, A. (2015). Leaf-gas exchange of five tree species at urban street sites. *Arboriculture & Urban Forestry*, *41*(3). https://doi.org/10.48044/jauf.2015.012

Gonfiantini, R., Gratziu, S., & Tongiorgi, E. (1965). Oxygen isotopic composition of water in leaves. In *Isotopes and radiation in soil-plant nutrition studies* (pp. 405–410). International Atomic Energy Agency. https://pascal-francis.inist.fr/vibad/index.php?action=getrecorddetail&idt=geodebrgm6905001181

Gorski, G., Strong, C., Good, S. P., Bares, R., Ehleringer, J. R., & Bowen, G. J. (2015). Vapor hydrogen and oxygen isotopes reflect water of combustion in the urban atmosphere. *Proceedings of the National Academy of Sciences of the United States of America*, *112*(11), 3247–3252. https://doi.org/10.1073/pnas.1424728112

Griffis, T. J., Wood, J. D., Baker, J. M., Lee, X., Xiao, K., Chen, Z., Welp, L. R., Schultz, N. M., Gorski, G., Chen, M., & Nieber, J. (2016). Investigating the source, transport, and isotope composition of water vapor in the planetary boundary layer. *Atmospheric Chemistry and Physics*, *16*(8), 5139–5157. https://doi.org/10.5194/acp-16-5139-2016

Grimm, N. B., Faeth, S. H., Golubiewski, N. E., Redman, C. L., Wu, J., Bai, X., & Briggs, J. M. (2008). Global change and the ecology of cities. *Science*, *319*(5864), 756–760. https://doi.org/10.1126/science.1150195

Gunawardena, K. R., Wells, M. J., & Kershaw, T. (2017). Utilising green and bluespace to mitigate urban heat Island intensity. *The Science of the Total Environment*, *584-585*, 1040–1055. https://doi.org/10.1016/j.scitotenv.2017.01.158

Guo, D. (2022). *Modelling Actual, Potential and Reference Crop: Package 'Evapotranspiration'*. https://cran.rstudio.com/web/packages/Evapotranspiration/Evapotranspiration.pdf

Herbstritt, B., Gralher, B., Seeger, S., Rinderer, M., & Weiler, M. (2022). Technical note: Mobile, discrete in situ vapor sampling for measurements of matrix-bound water stable isotopes. *Hydrology and Earth System Sciences*, 1–31. https://doi.org/10.5194/hess-2022-393

Horita, J., Rozanski, K., & Cohen, S. (2008). Isotope effects in the evaporation of water: A status report of the Craig-Gordon model. *Isotopes in Environmental and Health Studies*, *44*(1), 23–49. https://doi.org/10.1080/10256010801887174

Hughes, C. E., & Crawford, J. (2012). A new precipitation weighted method for determining the meteoric water line for hydrological applications demonstrated using Australian and global GNIP data. *Journal of Hydrology*, *464-465*, 344–351. https://doi.org/10.1016/j.jhydrol.2012.07.029

Keeling, C. D. (1958). The concentration and isotopic abundances of atmospheric carbon dioxide in rural areas. *Geochimica et Cosmochimica Acta*, *13*(4), 322–334. https://doi.org/10.1016/0016-7037(58)90033-4

Keesstra, S., Nunes, J., Novara, A., Finger, D., Avelar, D., Kalantari, Z., & Cerdà, A. (2018). The superior effect of nature based solutions in land management for enhancing ecosystem services. *The Science of the Total Environment*, *610-611*, 997–1009. https://doi.org/10.1016/j.scitotenv.2017.08.077

Kool, D., Agam, N., Lazarovitch, N., Heitman, J. L., Sauer, T. J., & Ben-Gal, A. (2014). A review of approaches for evapotranspiration partitioning. *Agricultural and Forest Meteorology*, *184*, 56–70. https://doi.org/10.1016/j.agrformet.2013.09.003

Kowarik, I. (2011). Novel urban ecosystems, biodiversity, and conservation. *Environmental Pollution*, *159*(8–9), 1974–1983. https://doi.org/10.1016/j.envpol.2011.02.022

Kruskal, W. H., & Wallis, W. A. (1952). Use of ranks in one-criterion variance analysis. *Journal of the American Statistical Association*, *47*(260), 583. https://doi.org/10.2307/2280779

Kuhlemann, L.-M., Tetzlaff, D., Smith, A., Kleinschmit, B., & Soulsby, C. (2021). Using soil water isotopes to infer the influence of contrasting urban green space on ecohydrological partitioning. *Hydrology and Earth System Sciences*, *25*(2), 927–943. https://doi.org/10.5194/hess-25-927-2021

Kunz, J., Räder, A., & Bauhus, J. (2016). Effects of drought and rewetting on growth and gas exchange of minor European broadleaved tree species. *Forests*, *7*(12), 239. https://doi.org/10.3390/f7100239

Kuppel, S., Tetzlaff, D., Maneta, M. P., & Soulsby, C. (2018). EcH$_2$O-iso 1.0: Water isotopes and age tracking in a process-based, distributed ecohydrological model. *Geoscientific Model Development*, *11*(7), 3045–3069. https://doi.org/10.5194/gmd-11-3045-2018

Landgraf, J., Tetzlaff, D., Dubbert, M., Dubbert, D., Smith, A., & Soulsby, C. (2022). Xylem water in riparian willow trees (Salix alba) reveals shallow sources of root water uptake by in situ monitoring of stable water isotopes. *Hydrology and Earth System Sciences*, *26*(8), 2073–2092. https://doi.org/10.5194/hess-26-2073-2022

Landwehr, J. M., & Coplen, T. (2006). Line-conditioned excess: A new method for characterizing stable hydrogen and oxygen isotope ratios in hydrologic systems.

Laonamsai, J., Ichiyanagi, K., Patsinghasanee, S., & Kamdee, K. (2021). Controls on stable isotopic characteristics of water vapour over Thailand. *Hydrological Processes*, *35*(7), 14202. https://doi.org/10.1002/hyp.14202

Lee, X., Sargent, S., Smith, R., & Tanner, B. (2005). In situ measurement of the water vapor 18O/16O isotope ratio for atmospheric and ecological applications. *Journal of Atmospheric and Oceanic Technology*, *22*(5), 555–565. https://doi.org/10.1175/JTECH1719.1

Lee, X., Smith, R., & Williams, J. (2006). Water vapour $^{18}O/^{16}O$ isotope ratio in surface air in New England, USA. *Tellus B: Chemical and Physical Meteorology*, *58*(4), 293. https://doi.org/10.1111/j.1600-0889.2006.00191.x

Lekshmy, P. R., Midhun, M., & Ramesh, R. (2018). Influence of stratiform clouds on δD and δ18O of monsoon water vapour and rain at two tropical coastal stations. *Journal of Hydrology*, *563*, 354–362. https://doi.org/10.1016/j.jhydrol.2018.06.001

Li, Y., An, W., Pang, H., Wu, S.-Y., Tang, Y., Zhang, W., & Hou, S. (2020). Variations of stable isotopic composition in atmospheric water vapor and their controlling factors—A 6-year continuous sampling study in Nanjing, eastern China. *Journal of Geophysical Research: Atmospheres*, *125*(22), 1697. https://doi.org/10.1029/2019JD031697

Li, Y., Riedl, A., Eugster, W., Buchmann, N., Cernusak, L. A., Lehmann, M. M., Werner, R. A., & Aemisegger, F. (2023). The role of radiative cooling and leaf wetting in air–leaf water exchange during dew and radiation fog events in a temperate grassland. *Agricultural and Forest Meteorology*, *328*, 109256. https://doi.org/10.1016/j.agrformet.2022.109256

Magh, R.-K., Gralher, B., Herbstritt, B., Kübert, A., Lim, H., Lundmark, T., & Marshall, J. (2022). Technical note: Conservative storage of water vapour – Practical in situ sampling of stable isotopes in tree stems. *Hydrology and Earth System Sciences*, *26*(13), 3573–3587. https://doi.org/10.5194/hess-26-3573-2022

Majoube, M. (1971). Fractionnement en oxygène 18 et en deutérium entre l'eau et sa vapeur. *Journal de Chimie Physique*, *68*, 1423–1436. https://doi.org/10.1051/jcp/1971681423

Marshall, D. C. (1958). Measurement of sap flow in conifers by heat transport. *Plant Physiology*, *33*, 385–396.

Marx, C., Tetzlaff, D., Hinkelmann, R., & Soulsby, C. (2022). Seasonal variations in soil–plant interactions in contrasting urban green spaces: Insights from water stable isotopes. *Journal of Hydrology*, *612*, 127998. https://doi.org/10.1016/j.jhydrol.2022.127998

Meili, N., Manoli, G., Burlando, P., Carmeliet, J., Chow, W. T., Coutts, A. M., Roth, M., Velasco, E., Vivoni, E. R., & Fatichi, S. (2021). Tree effects on urban microclimate: Diurnal, seasonal, and climatic temperature differences explained by separating radiation, evapotranspiration, and roughness effects. *Urban Forestry & Urban Greening*, *58*, 126970. https://doi.org/10.1016/j.ufug.2020.126970

Mercer, J. J., Liefert, D. T., & Williams, D. G. (2020). Atmospheric vapour and precipitation are not in isotopic equilibrium in a continental mountain environment. *Hydrological Processes*, *34*(14), 3078–3101. https://doi.org/10.1002/hyp.13775

Moreira, M., Sternberg, L., Martinelli, L., Victoria, R., Barbosa, E., Bonates, L., & Nepstad, D. (1997). Contribution of transpiration to forest ambient vapour based on isotopic measurements. *Global Change Biology*, *3*(5), 439–450. https://doi.org/10.1046/j.1365-2486.1997.00082.x

Norton, B. A., Bending, G. D., Clark, R., Corstanje, R., Dunnett, N., Evans, K. L., Grafius, D. R., Gravestock, E., Grice, S. M., Harris, J. A., Hilton, S., Hoyle, H., Lim, E., Mercer, T. G., Pawlett, M., Pescott, O. L., Richards, J. P., Southon, G. E., & Warren, P. H. (2019). Urban meadows as an alternative to short mown grassland: Effects of composition and height on biodiversity. *Ecological Applications: A Publication of the Ecological Society of America*, *29*(6), e01946. https://doi.org/10.1002/eap.1946

Oerter, E. J., & Bowen, G. (2017). In situ monitoring of H and O stable isotopes in soil water reveals ecohydrologic dynamics in managed soil systems. *Ecohydrology*, *10*(4), e1841. https://doi.org/10.1002/eco.1841

Penchenat, T., Vimeux, F., Daux, V., Cattani, O., Viale, M., Villalba, R., Srur, A., & Outrequin, C. (2020). Isotopic equilibrium between precipitation and water vapor in northern Patagonia and its consequences on δ 18 O cellulose estimate. *Journal of Geophysical Research: Biogeosciences*, *125*(3), 5418. https://doi.org/10.1029/2019JG005418

Ponte, S., Sonti, N. F., Phillips, T. H., & Pavao-Zuckerman, M. A. (2021). Transpiration rates of red maple (Acer rubrum L.) differ between management contexts in urban forests of Maryland, USA. *Scientific Reports*, *11*(1), 22538. https://doi.org/10.1038/s41598-021-01804-3

Rothfuss, Y., Merz, S., Vanderborght, J., Hermes, N., Weuthen, A., Pohlmeier, A., Vereecken, H., & Brüggemann, N. (2015). Long-term and high-frequency non-destructive monitoring of water stable isotope profiles in an evaporating soil column. *Hydrology and Earth System Sciences*, *19*(10), 4067–4080. https://doi.org/10.5194/hess-19-4067-2015

Rothfuss, Y., Quade, M., Brüggemann, N., Graf, A., Vereecken, H., & Dubbert, M. (2021). Reviews and syntheses: Gaining insights into evapotranspiration partitioning with novel isotopic monitoring methods. *Biogeosciences*, *18*(12), 3701–3732. https://doi.org/10.5194/bg-18-3701-2021

Schirmer, M., Leschik, S., & Musolff, A. (2013). Current research in urban hydrogeology – A review. *Advances in Water Resources*, *51*, 280–291. https://doi.org/10.1016/j.advwatres.2012.06.015

SenUVK. (2018). *Natura 2000 Berlin*. https://www.berlin.de/sen/uvk/natur-und-gruen/naturschutz/natura-2000/natura-gebiete/wasserwerk-friedrichshagen/

SenUVK. (2019a). *Grünflächeninformationssystem (GRIS): Anteil öffentlicher Grünflächen in Berlin*. https://www.berlin.de/senuvk/umwelt/stadtgruen/gruenanlagen/de/daten_fakten/downloads/ausw_5.pdf

SenUVK. (2019b). *Grünflächeninformationssystem (GRIS): Öffentliche Grünflächen in Berlin – Flächenübersicht der Bezirke*. https://www.berlin.de/sen/uvk/_assets/natur-gruen/stadtgruen/daten-und-fakten/ausw_13.pdf

Shapiro, S. S., & Wilk, M. B. (1965). An analysis of variance test for normality (complete samples). *Biometrika*, *52*(3/4), 591. https://doi.org/10.2307/2333709

Shashua-Bar, L., Pearlmutter, D., & Erell, E. (2011). The influence of trees and grass on outdoor thermal comfort in a hot-arid environment. *International Journal of Climatology*, *31*(10), 1498–1506. https://doi.org/10.1002/joc.2177

Singer, M. B., Asfaw, D. T., Rosolem, R., Cuthbert, M. O., Miralles, D. G., MacLeod, D., Quichimbo, E. A., & Michaelides, K. (2021). Hourly potential evapotranspiration at 0.1° resolution for the global land surface from 1981-present. *Scientific Data*, *8*(1), 224. https://doi.org/10.1038/s41597-021-01003-9

Smith, A., Tetzlaff, D., Landgraf, J., Dubbert, M., & Soulsby, C. (2022). Modelling temporal variability of in situ soil water and vegetation isotopes reveals ecohydrological couplings in a riparian willow plot. *Biogeosciences*, *19*(9), 2465–2485. https://doi.org/10.5194/bg-19-2465-2022

Spearman, C. (1904). "general intelligence," objectively determined and measured. *The American Journal of Psychology*, *15*(2), 201. https://doi.org/10.2307/1412107

Stackebrandt, W., & Manhenke, V. (2010). *Geologie und geopotenziale in Brandenburg: Atlas zur Geologie von Brandenburg*. Cottbus.

Steen-Larsen, H. C., Johnsen, S. J., Masson-Delmotte, V., Stenni, B., Risi, C., Sodemann, H., Balslev-Clausen, D., Blunier, T., Dahl-Jensen, D., Ellehøj, M. D., Falourd, S., Grindsted, A., Gkinis, V., Jouzel, J., Popp, T., Sheldon, S., Simonsen, S. B., Sjolte, J., Steffensen, J. P., … White, J. W. C. (2013). Continuous monitoring of summer surface water vapor isotopic composition above the Greenland ice sheet. *Atmospheric Chemistry and Physics*, *13*(9), 4815–4828. https://doi.org/10.5194/acp-13-4815-2013

Stevenson, J. L., Birkel, C., Comte, J.-C., Tetzlaff, D., Marx, C., Neill, A., Maneta, M., Boll, J., & Soulsby, C. (2023). Quantifying heterogeneity in ecohydrological partitioning in urban green spaces through the integration of empirical and modelling approaches. *Environmental Monitoring and Assessment*, *195*(4), 468. https://doi.org/10.1007/s10661-023-11055-6

Stevenson, J. L., Geris, J., Birkel, C., Tetzlaff, D., & Soulsby, C. (2022). Assessing land use influences on isotopic variability and stream water ages in urbanising rural catchments. *Isotopes in Environmental and Health Studies*, *58*(3), 277–300. https://doi.org/10.1080/10256016.2022.2070615

Student. (1908). The probable error of a mean. *Biometrika*, *6*(1), 1. https://doi.org/10.2307/2331554

Tetzlaff, D., Buttle, J., Carey, S. K., Kohn, M. J., Laudon, H., McNamara, J. P., Smith, A., Sprenger, M., & Soulsby, C. (2021). Stable isotopes of water reveal differences in plant – Soil water relationships across northern environments. *Hydrological Processes*, *35*(1), 10423. https://doi.org/10.1002/hyp.14023

Tetzlaff, D., Buttle, J., Carey, S. K., van Huijgevoort, M. H. J., Laudon, H., McNamara, J. P., Mitchell, C. P. J., Spence, C., Gabor, R. S., & Soulsby, C. (2015). A preliminary assessment of water partitioning and ecohydrological coupling in northern headwaters using stable isotopes and conceptual runoff models. *Hydrological Processes*, *29*(25), 5153–5173. https://doi.org/10.1002/hyp.10515

Tremoy, G., Vimeux, F., Cattani, O., Mayaki, S., Souley, I., & Favreau, G. (2011). Measurements of water vapor isotope ratios with wavelength-scanned cavity ring-down spectroscopy technology: New insights and important caveats for deuterium excess measurements in tropical areas in comparison with isotope-ratio mass spectrometry. *Rapid Communications in Mass Spectrometry*, *25*(23), 3469–3480. https://doi.org/10.1002/rcm.5252

Vimeux, F., & Risi, C. (2021). Isotopic equilibrium between raindrops and water vapor during the onset and the termination of the 2005–2006 wet season in the Bolivian Andes. *Journal of Hydrology*, *598*, 126472. https://doi.org/10.1016/j.jhydrol.2021.126472

Walker, C. D., & Brunel, J.-P. (1990). Examining evapotranspiration in a semi-arid region using stable isotopes of hydrogen and oxygen. *Journal of Hydrology*, *118*(1–4), 55–75. https://doi.org/10.1016/0022-1694(90)90250-2

Wang, C., Wang, Z.-H., & Yang, J. (2018). Cooling effect of urban trees on the built environment of contiguous United States. *Earth's Future*, *6*(8), 1066–1081. https://doi.org/10.1029/2018EF000891

Wei, Z., Lee, X., Aemisegger, F., Benetti, M., Berkelhammer, M., Casado, M., Caylor, K., Christner, E., Dyroff, C., García, O., González, Y., Griffis, T., Kurita, N., Liang, J., Liang, M. C., Lin, G., Noone, D., Gribanov, K., Munksgaard, N. C., … Yoshimura, K. (2019). A global database of water vapor isotopes measured with high temporal resolution infrared laser spectroscopy. *Scientific Data*, *6*, 180302. https://doi.org/10.1038/sdata.2018.302

Wei, Z., Yoshimura, K., Okazaki, A., Kim, W., Liu, Z., & Yokoi, M. (2015). Partitioning of evapotranspiration using high-frequency water vapor isotopic measurement over a rice paddy field. *Water Resources Research*, *51*(5), 3716–3729. https://doi.org/10.1002/2014WR016737

Werner, C., Schnyder, H., Cuntz, M., Keitel, C., Zeeman, M. J., Dawson, T. E., Badeck, F. W., Brugnoli, E., Ghashghaie, J., Grams, T. E. E., Kayler, Z. E., Lakatos, M., Lee, X., Máguas, C., Ogée, J., Rascher, K. G., Siegwolf, R. T. W., Unger, S., Welker, J., … Gessler, A. (2012). Progress and challenges in using stable isotopes to trace plant carbon and water relations across scales. *Biogeosciences*, *9*(8), 3083–3111. https://doi.org/10.5194/bg-9-3083-2012

Wilcoxon, F. (1945). Individual comparisons by ranking methods. *Biometrics Bulletin*, *1*(6), 80. https://doi.org/10.2307/3001968

Willis, K. J., & Petrokofsky, G. (2017). The natural capital of city trees. *Science*, *356*, 374–376. https://doi.org/10.1126/science.aam9724

Xu, T., Pang, H., Zhan, Z., Zhang, W., Guo, H., Wu, S., & Hou, S. (2022). Water vapor isotopes indicating rapid shift among multiple moisture sources for the 2018–2019 winter extreme precipitation events in southeastern China. *Hydrology and Earth System Sciences*, *26*(1), 117–127. https://doi.org/10.5194/hess-26-117-2022

Yakir, D., & Sternberg, L. S. L. (2000). The use of stable isotopes to study ecosystem gas exchange. *Oecologia*, *123*(3), 297–311. https://doi.org/10.1007/s004420051016

SUPPORTING INFORMATION

Additional supporting information can be found online in the Supporting Information section at the end of this article.

How to cite this article: Ring, A.-M., Tetzlaff, D., Dubbert, M., Dubbert, D., & Soulsby, C. (2023). High-resolution in situ stable isotope measurements reveal contrasting atmospheric vapour dynamics above different urban vegetation. *Hydrological Processes*, *37*(9), e14989. https://doi.org/10.1002/hyp.14989